Comprehensive Joint Time-Frequency Analysis toward Condition Based Maintenance Regimes for Electrical and Mechanical Components

David Coats

July 2012

Abstract

Based upon a framework of time-frequency analysis, a path towards systematic and comprehensive implementation of condition based maintenance (CBM), or maintenance only upon evidence of need, is outlined for both electrical and mechanical systems. Specifically, metrics are proposed for helicopter drivetrain systems and electrical cable. Using principles of time-frequency analysis, metrics for health assessment in non-destructive and non-invasive tests provide a basis for diagnostic and prognostic analysis. A form of Rényi entropy or Rényi information based mutual information measure is proposed for comparing vibration data from multiple sensors toward the creation of new condition indicators for use in rotorcraft. Using similar methodology, a process for non-invasively assessing the health of low voltage instrumentation cables and medium to high voltage feeder and transmission cables is proposed by way of Joint Time-frequency Domain Reflectometry (JTFDR).

From this starting point of derived health indicators for separate systems, research is proposed to facilitate the practical implementation of such technology. A new concept of non-parametric signal detection and classification technique is proposed using mutual information measures in the time-frequency domain. The time-frequency based self and mutual information is defined in terms of the cross time-frequency distribution. Based on time-frequency mutual information theory, this paper presents applications of the proposed technique to real-world vibration data obtained from a dedicated condition based maintenance experimental testbed. Baseline, unbalanced, and misaligned experimental settings of helicopter drive train bearings and shafts are quantitatively distinguished by the proposed techniques. With unbalance quantifiable by variance in the in-phase mutual information and misalignment quantifiable by variance in the quadrature mutual information developed and presented herein, machine health classification can be accomplished by use of statistical bounding regions.

Electrical, reflectometry-based methods of health evaluation are proposed and will be compared to existing methods of high voltage test such as high voltage withstand and partial discharge, which can be destructive when applied to cables. Surface wave insulation health assessment is proposed as a means of connecting to a cable under test in a noninvasive manner. Also, toward a new standard of smart grid active condition based maintenance strategies, joint time-frequency domain reflectometry is proposed for monitoring the health of high temperature super- conducting (HTS) cable. Conditions of localized impedance fluctuation due to coolant leak have been simulated with the reflectometry assessment properly detecting minute changes in cable impedance and indicating location and severity of faulted segments.

Contents

1 Introduction

1.1 Preventative Maintenance Concept and Analysis

Standard maintenance practices in most industries involve replacing existing parts after a certain time period or a certain number of operational hours. This practice is called time-based maintenance (TBM) and can lead to unexpected failures in critical parts due to unexpected wear and unforeseen physical stresses, causing operational downtime and potential safety hazards [1]. Therefore, instead of TBM, it is desirable to consider use-based maintenance practices so that critical parts are replaced or repaired before their full lifetimes on a variable basis balancing and optimizing both economic and safe operating conditions [2]. Concepts of condition-based maintenance will be applied to health monitoring of rotorcraft and rotational electromechanical systems as well as power instrumentation and distribution, or to generalize further, cable systems.

A new practice of condition-based maintenance (CBM) is proposed for military aviation fleet management which fits within the existing framework of vibration management presented by the army's Vibration Management Enhancement Program (VMEP) and Health Usage Monitoring System (HUMS) infrastructure or could be separated into its own stand-alone product. For health assessment and management of cable systems, new theory and applied examples are posited for Joint Time-Frequency Domain Reflectometry (JTFDR) to help realize a practical implementation of the technology. The overarching goal of both research topics is advancing the time- and reaction-based maintenance schedules typically offered in electrical and mechanical systems toward ones that are predictive and proactive [3, 4].

A typical course of action toward this overarching goal of generalized condition-based maintenance is presented herein to establish the background for unified condition-based maintenance strategies which could be used in systems with complicated electrical and mechanical systems such as helicopter drivetrain systems, wind farm systems, nuclear instrumentation and control fuel rod systems, and high voltage, high temperature super conducting (HTS) generation/distribution systems. To achieve this innovative maintenance practice, data must be collected from vital operational components and analyzed in order to determine the current (diagnostic) state of the baseline case and later the future (prognostic) health of these same critical components. Further, aging or conditioning must be simulated in a controlled testbed and monitored to identify progressive degradation trends using heath assessment metrics. These testbed trends can be compared to existing historical component data from active articles, where such data is available, to form characteristic prognostic functions. Once effective diagnostic and prognostic health assessment monitoring models are created condition indicator (CI) or health indicator (HI) single or multiple dimensional metrics can be gathered and packaged into a monitoring unit. The proposed research will focus on developing metrics for health assessment of rotational components in helicopter drivetrain systems from an existing testbed and developing an accelerated aging testbed for instrumentation and medium voltage distribution systems with a practical implementation of non-invasive insulation health monitoring.

1.2 Health Monitoring of Rotorcraft Drivetrain

In order to monitor the health status of drivetrain systems, a variety of signals are collected, including vibration [5, 6], acoustic [7], and temperature. Over the past decade great advancements have been made in health diagnostics and vibration management in military helicopters in terms of both progression of metric indicators and cost benefits to the US Army helicopter fleet maintainers [1]-[4]. The successes to date have resulted in the large-scale deployment of increasingly useful health monitoring systems such as HUMS (Health and Usage Monitoring Systems) using Vibration Management Enhancement Program (VMEP) hardware, which have generated a wide range of benefits from increased safety to reduced maintenance costs.

Most CBM tools such as HUMS for Apache and Blackhawk helicopters assist machinery maintainers in identifying faulted components through the use of simple visual interfaces and indicators. The most commonly

utilized functions are condition indicators (CI), which output a dimensioned or dimensionless single scalar value to monitor key factors most frequently related to frequency analysis of vibration signature. Condition indicators need not be based upon vibration analysis alone and may include component temperatures or acoustic data for separate or fused CIs. Examples of common indicators in machine diagnostics and prognostics include: spectral peak analysis, envelope analysis, energy ratio, crest factor, sideband index, and kurtosis of residual signals [8]. These CI values are typically compared with pre-established thresholds in a simple decision tree classifier which assign the CI some form of ranked class such as "Good," "Caution," or "Exceeded," and these classes are then utilized by maintainers in vital decision-making processes. A given component can have several CIs which may additively form a health indicator (HI). Typically, CIs or HIs are not fault-specific; multiple fault types can affect the value of a single CI, and a single fault could affect multiple CIs.

While various condition and health indicators do exist, the proposed work improves their effectiveness by developing new general methods for fault analysis based around time-frequency analysis that could be used in existing or new CIs for indication of machinery failure. Previous studies on CBM from diverse applications [9, 10] have shown that abnormality of the system is characterized by transient precursors in the signals. Through their use in detecting transient precursors, advanced signal processing techniques have contributed to develop diagnostics and prognostics algorithms for aging aircraft [11]. The classical methods for vibration analysis such as spectral analysis or time-frequency distributions represent frequency- or time- and frequency-localized energy, however, it is not expedient to analyze multiple signals that have been simultaneously collected from systems under test. In particular, time-frequency analysis is extremely useful to analyze the transient signature of the abnormality and its precursors [12]. Previous convention dictated that time-frequency based applications were difficult to implement in real-time, however, methods [14] have been proposed to accomplish time-frequency algorithms feasible for the constant monitoring required for CBM [15]. We present a path toward using time-frequency analysis and specified metrics based on time-frequency representations for condition and health monitoring, advancing the analysis of data from existing condition monitoring systems without the use of additional hardware.

We propose a new concept of non-parametric detection and classification of signals. We define time-frequency based self and mutual information in order to classify the health status of the system components in Section 2.5-2.7. Other methods [6], [16], [17] have been proposed to use either classical methods or neoclassical methods moving toward the use of both time- and frequency- based information. The proposed method takes advantage of both time- and frequency- domain transients to establish a complexity measurement for potential assessment of component health. The experimental setup and data description are provided in Section 3. The results and discussions are provided in Section 3.4, and conclusions of the paper are drawn in Section 5. Based on the time-frequency based mutual information theory, this paper presents applications of the proposed technique to the real-world vibration data and a path for future research in Section 6.1.

1.3 Health Monitoring of Electric Cable

The state of the art for non-destructive detection of defects in wiring and cable is divided into two categories: time-domain reflectometry (TDR) and frequency-domain reflectometry (FDR). Although these techniques can successfully assess hard defects, they fall short in the detection and location of soft defects, an essential prognostic capability. The limitations of both TDR and FDR are caused by ineffective design of reference signal and inappropriate processing of the reflected signal in TDR and FDR, in that these methods refer to only the time or frequency domains, but not both. We seek an innovative, optimal type of reflectometry that simultaneously uses the time and frequency domains: Joint Time-Frequency Domain Reflectometry (JTFDR). The JTFDR technique exhibits its efficacy in cable diagnostics and prognostics such as communication, electric power, and nuclear control and instrumentation (C and I) cables [32].

In searching for a more universal method of signal injection for reflectometry-based assessment, particularly in cases of prognostic remaining useful life indicators, we sought a method that could couple to the cable in question (1) without requiring removal of the cable under test from a given system, (2) without damaging instrumentation or transmission cables, and (3) sensitive enough to enable assessment of impedance of the cable by reflectometry. In surveying options of implementation in these three key areas, we desired a means to further adjust the optimal reference to account for non-idealities in the frequency response of the injection

method. In this report we will focus on the theory of surface wave injection of reflectometry signals, a method for optimizing a reflectometry signal in time and frequency domains, and practical optimizations in narrowband segments or slices of a larger bandwidth. These efforts will cumulatively add to the assessment of health assessment of insulation materials in the real-world electric power systems.

2 Theory of Joint Time-Frequency Analysis

The goal of this section is to establish some necessary theoretical background for the time-frequency applications addressed in this proposal. Time-frequency analysis will be addressed as it applies in the following two applications: the time-frequency cross correlation which forms the base for JTFDR reflectometry which will be applied in the health monitoring of electric cables and the time-frequency mutual information measure which will be used in health monitoring of helicopter drivetrains.

2.1 Joint Time-Frequency Domain Reflectometry Optimal Reference

To produce an optimal reference signal we must optimize a balance between time domain resolution and frequency domain resolution. In order to optimize the resolution in both domains, we consider a signal that satisfies the uncertainty principle (derived from the product of time and bandwidth variances and meeting the Cauchy-Schwarz inequality). In this, case we have chosen a Gaussian envelope due to its functionality as an eigenfunction of the Fourier transform and its similar variance in both the time and frequency domain. This Gaussian envelope encloses a chirp signal which provides a specified frequency bandwidth and the overall equation is provided below:

$$s(t) = \left(\frac{\alpha}{\pi}\right)^{1/4} e^{-\frac{\alpha(t-t_0)^2}{2} + j\frac{\beta(t-t_0)^2}{2} + j\omega_0(t-t_0)} \tag{1}$$

Additionally, the use of the Gaussian envelope provides the added benefit of having well-established background in general statistics and statistical signal processing of jointly random bivariate distributions. In proposed research Gaussian properties typically used for statistical hypothesis tests will be used for identification of envelope center and outer boundaries (used in detection of fault location and automated determination of optimized reference). In this study, we will work with the function under the simplifying assumption that time center t_0 is neglected (or centered at zero). This yields the following equation:

$$s(t) = \left(\frac{\alpha}{\pi}\right)^{1/4} e^{-\frac{\alpha t}{2} + j\frac{\beta t^2}{2} + j\omega_0 t} \tag{2}$$

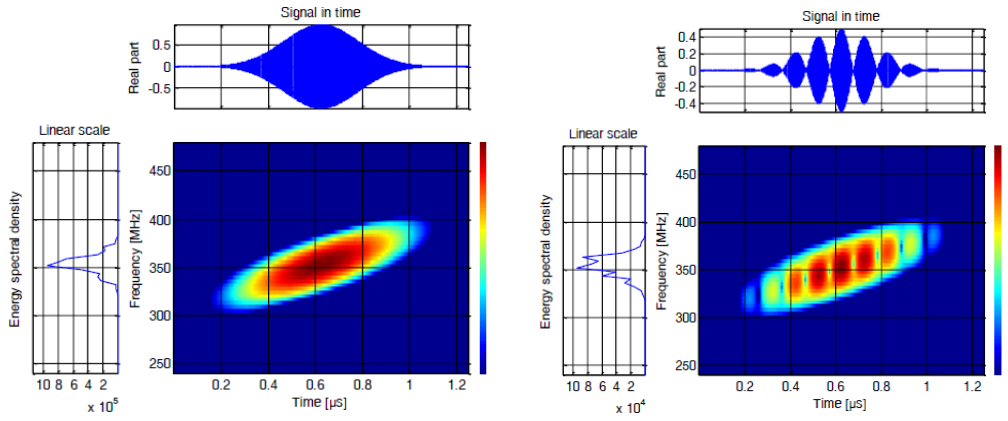

(a) (b)

Figure 1: Time-frequency distribution of (a) optimal reference and (b) reference with sinusoidal modulation

2.2 Time-Frequency Distribution

All time-frequency distributions can be obtained from the definition of Cohen's class:

$$TFD_x(t,\omega;\phi) = \frac{1}{4\pi^2}\int\int\int x^*(u-\frac{\tau}{2})x(u+\frac{\tau}{2})\phi(\theta,\tau)e^{-j\theta t-j\tau\omega+j\theta u}d\theta d\tau du \tag{3}$$

Where $x(t)$ is the analytic representation of a signal, $x^*(t)$ is the complex conjugate of $x(t)$, and $\phi(\theta,\tau)$ is a two-dimensional function known as a kernel. The choice of kernel has an effect on marginals, total energy, realness, time shift, frequency modulation, scaling invariance, and cross term minimization [22]. Among the various types of time-frequency distributions, the wigner ville (WV) distribution, Choi-Williams (CW) distribution, and reduced interference distribution (RID) have been shown to exhibit the most suitable properties for the analysis of the time-varying frequency characteristics of a disturbance or provide the most common solution to the time frequency kernel selection. For this preliminary analysis we will consider the selection of these three kernels along with Zhao-Atlas-Marks (ZAM) kernel to see which kernel performs the best for vibration signal analysis. The kernels for the distributions are given as follows:

$$\phi(\theta,\tau)_{WV} = 1 \tag{4}$$

$$\phi(\theta,\tau)_{CW} = e^{\frac{-\theta^2\tau^2}{\sigma}} \tag{5}$$

$$\phi(\theta,\tau)_{ZAM} = g(\tau)|\tau|\frac{\sin a\theta\tau}{a\theta\tau} \tag{6}$$

Where $\phi(\theta,\tau)_{WV}$, $\phi(\theta,\tau)_{CW}$, and $\phi(\theta,\tau)_{ZAM}$ are kernels for WV, CW, and ZAM distributions, respectively. These Choi-Williams and Zhao-Atlas-Marks kernels may be classified generally as reduced interference distributions (RID) designed with the intent of reducing the "cross-terms" or inter-harmonic noise introduced by computation of the time-frequency distribution on multi-component signals. To obtain the time-frequency distribution of the optimal reference we take the Wigner Transform defined for a generic time-domain function, $s(t)$, as follows:

$$W(t,\omega) = \frac{1}{2\pi}\int_{-\infty}^{\infty} s^*(t-\frac{1}{2}\tau)\cdot s(t+\frac{1}{2}\tau)e^{-j\tau\omega}d\tau \tag{7}$$

We will consider the simple transform pair:

$$s(t) \rightleftharpoons W(t,\omega) \tag{8}$$

Time and frequency shift properties as provided by Cohen [35], show that for a time domain signal, $s(t)$, from 2 with a Wigner Transform given as the following bivariate distribution, $W(t,\omega)$, a shift in time and frequency given by:

$$s(t) \rightarrow e^{j\omega_0 t}s(t-t_0) \tag{9}$$

A subsequent shift in time and frequency is seen in the Wigner Distribution:

$$W(t,\omega) \rightarrow W_1(t-t_0,\omega-\omega_0) \tag{10}$$

Using this simplified assumption we can take the Wigner transform of the simplified optimal reference and form a derivation of this distribution:

$$W_s(t,\omega) = \frac{1}{2\pi}\left(\frac{\alpha}{\pi}\right)^{1/2}\int e^{-\frac{\alpha(t-\frac{1}{2}\tau)^2}{2}-j\frac{\beta(t-\frac{1}{2}\tau)^2}{2}-j\omega_0(t-\frac{1}{2}\tau)}\cdot e^{-\frac{\alpha(t+\frac{1}{2}\tau)^2}{2}+j\frac{\beta(t+\frac{1}{2}\tau)^2}{2}+j\omega_0(t+\frac{1}{2}\tau)}\cdot e^{j\tau\omega}\cdot d\tau \tag{11}$$

$$W_s(t,\omega) = \frac{1}{2\pi}(\frac{\alpha}{\pi})^{1/2}\int e^{-\frac{\alpha(t^2-\tau t+\frac{1}{4}\tau^2)}{2}-j\frac{\beta(t^2-\tau t+\frac{1}{4}\tau^2)}{2}-j\omega_0(t-\frac{1}{2}\tau)}\cdot e^{-\frac{\alpha(t^2+\tau t+\frac{1}{4}\tau^2)}{2}+j\frac{\beta(t^2+\tau t+\frac{1}{4}\tau^2)}{2}+j\omega_0(t+\frac{1}{2}\tau)}\cdot e^{j\tau\omega}\cdot d\tau \tag{12}$$

The improper integral can be manipulated into the following form for an express solution:

$$\int_{-\infty}^{\infty} e^{-(a\tau^2+b\tau+c)}d\tau = \sqrt{\frac{\pi}{a}}e^{\frac{b^2-4ac}{4a}} \tag{13}$$

Reexpressing the improper integral we obtain:

$$W_s(t,\omega) = \frac{1}{2\pi}\left(\frac{\alpha}{\pi}\right)^{1/2}\int_{-\infty}^{\infty} e^{-(\frac{1}{4}\alpha\tau^2+j(\omega-\beta t-\omega_0)\tau+\alpha t^2)}d\tau \tag{14}$$

Further simplifying, we obtain:

$$W_s(t,\omega) = \frac{1}{\pi}\cdot e^{\frac{(j(\omega-\beta t-\omega_0))^2-\alpha^2t^2}{\alpha}} \tag{15}$$

$$W_s(t,\omega) = \frac{1}{\pi}\cdot e^{\alpha t^2-\frac{(\omega-\beta t-\omega_0)^2}{\alpha}} \tag{16}$$

Now we will consider the same simplified signal in (2) and add a sinusoidal modulation component to the signal. The signal becomes:

$$s(t) = \left(\frac{\alpha}{\pi}\right)^{1/4} e^{-\frac{\alpha t}{2}+j\frac{\beta t^2}{2}+jm\cdot sin\omega_m t+j\omega_0 t} \tag{17}$$

With the following derivation for the Wigner transform

$$W_s(t,\omega) = \frac{1}{2\pi}\left(\frac{\alpha}{\pi}\right)^{1/2}\int e^{-\frac{\alpha(t-\frac{1}{2}\tau)^2}{2}-j\frac{\beta(t-\frac{1}{2}\tau)^2}{2}-jm\cdot sin\omega_m(t-\frac{1}{2}\tau)-j\omega_0(t-\frac{1}{2}\tau)}\cdot e^{-\frac{\alpha(t+\frac{1}{2}\tau)^2}{2}+j\frac{\beta(t+\frac{1}{2}\tau)^2}{2}+jm\cdot sin\omega_m(t+\frac{1}{2}\tau)+j\omega_0(t+\frac{1}{2}\tau)}\cdot e^{j\tau\omega}\cdot d\tau \tag{18}$$

$$W_s(t,\omega) = \frac{1}{2\pi}\left(\frac{\alpha}{\pi}\right)^{1/2}\int_{-\infty}^{\infty} e^{-(\frac{1}{4}\alpha\tau^2+jm\cdot(sin\omega_m(t-\frac{1}{2}\tau)-sin\omega_m(t+\frac{1}{2}\tau))+j(\omega-\beta t-\omega_0)\tau+\alpha t^2)}d\tau \tag{19}$$

$$W_s(t,\omega) = \frac{1}{2\pi}\left(\frac{\alpha}{\pi}\right)^{1/2}\int_{-\infty}^{\infty} e^{-(\frac{1}{4}\alpha\tau^2+j2\cdot m\cdot sin(\omega_m t)\cdot cos(\frac{\tau}{2})+j(\omega-\beta t-\omega_0)\tau+\alpha t^2)}d\tau \tag{20}$$

$$W_s(t,\omega) = \frac{1}{2\pi}\left(\frac{\alpha}{\pi}\right)^{1/2}e^{-\alpha t^2}\int_{-\infty}^{\infty} e^{-(\frac{1}{4}\alpha\tau^2+j2\cdot m\cdot sin(\omega_m t)\cdot cos(\frac{\tau}{2})+j(\omega-\beta t-\omega_0)\tau)}d\tau \tag{21}$$

$$e^{j2m\cdot sin(\omega_m t)\cdot cos(\frac{\tau}{2})} = \sum_{n=-\infty}^{\infty} J_n(2m\cdot cos(\omega_m t))e^{\frac{jn\omega_m\tau}{2}} \tag{22}$$

$$W_s(t,\omega) = \frac{1}{\pi}e^{-\alpha t^2}\sum_{n=-\infty}^{\infty} J_n(2m\cdot cos(\omega_m t))e^{\frac{(\omega-\omega_0-\beta t-\frac{n\omega_m}{2})^2}{\alpha}} \tag{23}$$

2.3 Numerical Approximation of Reference Signal for Embedded Implementation

For further background regarding the equation given in 23, we can further analyze the Bessel function described in 22. The Bessel function is the solution to the differential equation given in

$$x^2\frac{d^2y}{dx^2}+x\frac{dy}{dx}+(x^2-\alpha^2)y = 0 \tag{24}$$

And can be described by the following integral relation :

$$J_n(x) = \frac{1}{2\pi}\int_{-\pi}^{\pi} e^{-i(n\tau-x\cdot sin\tau)}d\tau \tag{25}$$

This equation presents a set of problems in that no closed-form representation exists for express solution. Operations such as cross-correlation (further described in Section 2.4) require numerical solutions and numerical approximations. Similarly in the case of the Fourier transform, a temporal integration is required. This allows for a number of different approximation methods which can be used in combination with an embedded sensor for constant or periodic health measurement and assessment. The simplest of the approximations is shown below:

$$J_0(x) \simeq \frac{2}{\pi}\int_0^1 \frac{cos(2n\delta\omega)}{\sqrt{1-\omega^2}} \tag{26}$$

Further potential methods for Bessel function approximation include Taylor series approximation, polynomial approximation, and exponential approximation. The Taylor series approximation [36] for $J_p(x)$ is given by the following summation:

$$J_p(x) = \sum_{m=0}^{\infty} t_{pm} x^{2m+p} \tag{27}$$

$$t_{pm} = \frac{(-1)^m}{2^{2m+p} m!(m+p)!} \tag{28}$$

To truncate the Taylor series to a given order x^n we can express the Taylor series as:

$$J_p^{T,n}(x) = \sum_{m=p}^{\frac{n+p}{2}} t_{p,m-p} x^{2m-p} \tag{29}$$

Alternatively a polynomial approximation [37] can be used such that:

$$J_0(x) \simeq \sum_{m=0}^{n} c_{nm} x^{2m} \tag{30}$$

$$c_{nm} = \frac{(-1)^m n^{1-2m(n+m-1)!}}{2^{2m}(n-m)!(m!)^2} \tag{31}$$

Lastly, an exponential approximation can be made. Due to the oscillatory nature of the Bessel function, for an exponential approximation to be made, the Bessel function must be represented as a set of complex exponentials [36]. This provides the following relationship:

$$J_V(x) = \frac{1}{2}\sum_{n=1}^{2N} a_n e^{s_n x} \tag{32}$$

where a_n, s_n are complex parameters such that $a_n = a_{nr} + j a_{ni}, s_n = s_{nr} + j s_{ni}$ and $a_{n+N} = a_n^*, s_{n+N} = s_n^*$. The zero order expansion is then given as:

$$J_0(x) = \frac{1}{2}\sum_{n=1}^{2N} a_n e^{s_n x} \tag{33}$$

These approximations can be used to make a simplified approximation of the optimized reference for implementation on smaller scale waveform generation and signal injection embedded systems toward eventual continuous or periodic health assessment monitoring in either cable insulation assessment or structural health monitoring.

2.4 Time-Frequency Cross Correlation

JTFDR computes the time-frequency cross correlation between an incident signal and the reflected signal through a propagating medium with the following equation:

$$C_{sr}(t) = \frac{1}{E_s E_r(t)} \int_{t'=t-T_s}^{t'=t+T_s} \int W_r(t',\omega) W_s(t'-t,\omega) d\omega dt' \tag{34}$$

where $W_r(t,\omega)$ is the Wigner distribution of the reflected signal; $W_s(t,\omega)$ is the Wigner distribution of incident signal; and E_s and $E_r(t)$ are normalization factors.

$$C_{sr}(t) = \frac{1}{E_s E_r(t)} \int_{t'=t-T_s}^{t'=t+T_s} \int e^{-\alpha(t')^2} \sum_{n=-\infty}^{\infty} J_n(2m \cdot cos(\omega_m t')) e^{\frac{(\omega-\omega_0-\beta t' - \frac{n\omega_m}{2})^2}{\alpha}} \cdot e^{-\alpha(t'-t)^2} \sum_{n=-\infty}^{\infty} J_n(2m \cdot cos(\omega_m(t'-t))) e^{\frac{(\omega-\omega_0-\beta(t'-t)-\frac{n\omega_m}{2})^2}{\alpha}} \tag{35}$$

2.5 Time-Frequency Rényi Information Measure

This section has been adapted from a previously submitted paper produced by the author [19]. The classical information measure of a continuous stochastic process is known as Shannon information [20] given as:

$$H_x = -\int_{-\infty}^{\infty} f(x) \log_2 f(x) dx \tag{36}$$

where the continuous function $f(x)$ is a probability density function which is positive and bounded between 0 and 1. Williams, Brown, and Hero proposed a measure of time-frequency information by use of the generalized Rényi information [20]. The definition of the generalized Rényi information [21] of a continuous bivariate distribution $P(x,y)$ is defined as follows:

$$H_\alpha(P) = \frac{1}{1-\alpha} \log_2 \frac{\int\int P^\alpha(x,y) dxdy}{\int\int P(x,y) dxdy} \tag{37}$$

The definition of the generalized Rényi information can be extended by replacing the bivariate distribution $P(x,y)$ with a Cohen's class [23] time-frequency distribution $C_s(t,\omega)$ of signal $s(t)$ with the following definition:

$$C_s(t,\omega;\phi) = \frac{1}{4\pi^2} \int\int\int s^*(u-\frac{\tau}{2}) s(u+\frac{\tau}{2}) * \phi(\theta,\tau) e^{-j\theta t - j\tau\omega + j\theta u} d\theta d\tau du \tag{38}$$

Use of the Cohen's class distribution permits a more general solution allowing for variable kernel selection. The kernel function of the distribution is described by the $\phi(\theta,\tau)$ term in (38). In other words, the theory described in this section presents analysis for the general case of the Cohen's class time-frequency distribution while any distribution kernel could be selected when applying the time-frequency mutual information measure including, but not limited to, the general (Cohen's class), spectrogram, Zhao-Atlas-Marks, Wigner-Ville, Choi-Williams, or reduced interference distribution (RID) kernel [23]. We selected the spectrogram kernel for the time-frequency information because it has the desirable property of nonnegativity forwarded by Williams, et.al in [20] for all time and frequency variables. To provide consistency of discussion with time-frequency analysis in Section **??**, the spectrogram here is defined as a Cohen's class distribution as seen in (38) where the kernel function $\phi(\theta,\tau)$ is specified as the spectrogram kernel given by:

$$\phi(\theta,\tau) = \int h^*(u-\frac{1}{2}\tau) h(u+\frac{1}{2}\tau) e^{-j\theta u} du \tag{39}$$

The order of the generalized Rényi information determined by parameter α for the time-frequency distribution has been investigated in [24] so that $\alpha = 3$ is a reasonable selection, with the exception of contrived counterexamples [20]. Hence, the following information measure of time-frequency distribution will be utilized:

$$H_\alpha(C_s) = \frac{1}{1-\alpha}\log_2 \frac{\int\int C_s^\alpha(t,\omega)dtd\omega}{\int\int C_s(t,\omega)dtd\omega} \tag{40}$$

2.6 Cross Time-Frequency Distribution

The metric $H_\alpha(C_s)$ defined in (40) measures the number of signal elements of $s(t)$ over the time and frequency planes. The Rényi information measure is a meaningful measure of time-frequency distribution, but it is only defined for a single realization of signal, e.g. self-information. If we have a pair of signals closely related, how can we define or quantify the interactions in terms of information? We will investigate a generalization of the time-frequency information measure by introducing the mutual time-frequency information.

In order to analyze the information of two closely spaced components, the classical mutual information of two random processes is extended to two time-frequency distribution functions. Let us consider the classical definition of the mutual information that might be extended to the measure of mutual information of the time-frequency distributions. The joint entropy $H(X,Y)$ of a pair of continuous random variables (X,Y) with a joint probability density function $p(x,y)$ is defined as:

$$H(X,Y) = -\int\int p(x,y)\log_2 p(x,y)dxdy \tag{41}$$

By chain rule,

$$H(X,Y) = H(X) + H(Y|X) \tag{42}$$

where $H(Y|X)$ is the conditional entropy. Under the same conditions, the mutual information $I(X;Y)$ is the relative entropy between the joint distribution $p(x,y)$ and the product distribution of the individual marginal distribution $p(x)$ and $p(y)$ as follows:

$$I(X;Y) = \int\int p(x,y)\log_2 \frac{p(x,y)}{p(x)\cdot p(y)} \tag{43}$$

The relation of the mutual information $I(X;Y)$ and joint entropy $H(X,Y)$ is defined as follows:

$$\begin{aligned} I(X;Y) &= H(X) - H(X|Y) \\ &= H(Y) - H(Y|X) \\ &= H(X) + H(Y) - H(X,Y) \end{aligned} \tag{44}$$

Thus, it is necessary for us to define cross time-frequency distribution $J_{s_1s_2}(t,\omega;\phi)$ of the signal pairs S_1 and S_2 [25].

$$\begin{aligned} J_{s_1s_2}(t,\omega;\phi) &= \frac{1}{4\pi^2}\int\int\int s_1(u+\frac{\tau}{2})s_2^*(u-\frac{\tau}{2})\phi(\theta,\tau) \\ &* \quad e^{-j\theta t - j\tau\omega + j\theta u}d\theta d\tau du \end{aligned} \tag{45}$$

The kernel $\phi(\theta,\tau)$ is equivalent to the kernel given in Cohen's class in (38) and the cross time-frequency distribution satisfies time and frequency marginal property under the same constraints given in Cohen's class. Consider a joint information of time-frequency distribution $H_\alpha(J_{s_1s_2})$ in terms of cross time-frequency distribution $J_{s_1s_2}(t,\omega;\phi)$ as follows:

$$\begin{aligned} H(S_1,S_2) &= H_\alpha(J_{s_1s_2}) = \\ &= -\frac{1}{1-\alpha}\log_2 \frac{\int\int J_{s_1s_2}^\alpha(t,\omega)dtd\omega}{\int\int J_{s_1s_2}(t,\omega)dtd\omega} \end{aligned} \tag{46}$$

2.7 Time-Frequency Mutual Information Measure

However, one must be careful in defining the information measure of the cross time-frequency distribution which is a complex number. In addition, normalization of the distribution is important for a proper bound of the information measure. Therefore, instead of direct application of the generalized Rényi information, consider the normalized cross time-frequency distribution $\overline{J}_{s_1s_2}(t,\omega)$ as follows:

$$\begin{aligned}
\overline{J}_{s_1s_2}(t,\omega) &= \frac{J_{s_1s_2}(t,\omega)}{\sqrt{C_{s_1}(t,\omega)\cdot C_{s_2}(t,\omega)}} \\
&= \frac{R_{s_1s_2}(t,\omega)}{\sqrt{C_{s_1}(t,\omega)\cdot C_{s_2}(t,\omega)}} \\
&+ j\frac{Q_{s_1s_2}(t,\omega)}{\sqrt{C_{s_1}(t,\omega)\cdot C_{s_2}(t,\omega)}} \\
&= \overline{R}_{s_1s_2}(t,\omega) + j\overline{Q}_{s_1s_2}(t,\omega) \qquad (47)
\end{aligned}$$

We can define the time-frequency mutual information measure of in-phase $I^R_\alpha(S_1;S_2) = -H_\alpha(\overline{R}_{s_1s_2})$ and quadrature $I^Q_\alpha(S_1;S_2) = -H_\alpha(\overline{Q}_{s_1s_2})$ as follows:

$$\begin{aligned}
I^R_\alpha(S_1;S_2) &= \frac{1}{1-\alpha}\log_2\int\int R^\alpha_{s_1s_2}(t,\omega)dtd\omega \\
&- \frac{1}{2}\cdot\{H_\alpha(C_{s_1}) + H_\alpha(C_{s_2})\} \qquad (48) \\
I^Q_\alpha(S_1;S_2) &= \frac{1}{1-\alpha}\log_2\int\int Q^\alpha_{s_1s_2}(t,\omega)dtd\omega \\
&- \frac{1}{2}\cdot\{H_\alpha(C_{s_1}) + H_\alpha(C_{s_2})\} \qquad (49)
\end{aligned}$$

Then, the mutual information measure $I_\alpha(S_1;S_2)$ of S_1 *and* S_2 is defined in terms of in-phase time-frequency mutual information $I^R_\alpha(S_1;S_2)$ and quadrature time-frequency mutual information $I^Q_\alpha(S_1;S_2)$ as follows:

$$\begin{aligned}
I_\alpha(S_1;S_2) &= I^R_\alpha(S_1;S_2) + I^Q_\alpha(S_1;S_2) \\
&= -H_\alpha(\overline{R}_{s_1s_2}) - H_\alpha(\overline{Q}_{s_1s_2}) \\
&= H_\alpha(C_{s_1}) - H_\alpha(C_{s_1}|C_{s_2}) \\
&= H_\alpha(C_{s_2}) - \underbrace{(H_\alpha(C_{s_1},C_{s_2}) - H_\alpha(C_{s_1}))}_{H_\alpha(C_{s_2}|C_{s_1})} \\
&= H_\alpha(C_{s_2}) - H_\alpha(C_{s_2}|C_{s_1}) \qquad (50)
\end{aligned}$$

Therefore, the mutual time-frequency information $I_\alpha(C_{s_1};C_{s_2})$ is the sum of individual time-frequency information $H_\alpha(C_{s_1})$, $H_\alpha(C_{s_2})$ and joint information $H_\alpha(C_{s_1},C_{s_2})$. For example, if $s_1(t) = s_2(t)$, then $C_{s_1} = C_{s_2}$ and $Q_{s_1s_2} = 0$ such that

$$I_\alpha(C_{s_1};C_{s_2}) = I_\alpha(C_{s_2};C_{s_2}) = H_\alpha(C_{s_1}) \quad \text{or} \quad H_\alpha(C_{s_2}) \qquad (51)$$

Based on the mutual time-frequency information measure, we investigate the efficacy of the proposed technique with real-world data sets. The experimental setup and data descriptions are provided in Section 3.

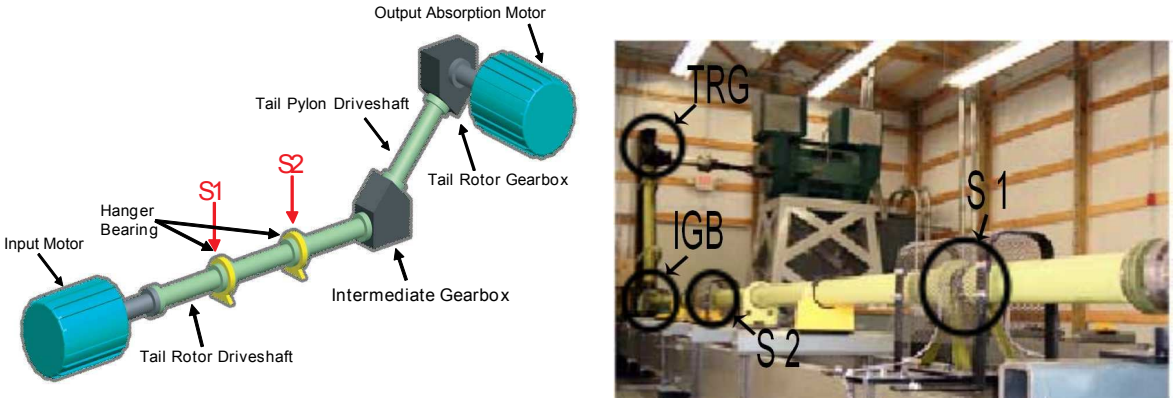

(a) (b)

Figure 2: Schematic representattion of AH-64 helicopter tail rotor drivetrain test stand (a) and actual test stand (b) with labeled components for comparison.

3 Health Monitoring of Rotorcraft Drivetrain by Mutual Information

3.1 Introduction

3.2 Experimental Setup

The CBM center at The University of South Carolina has an AH-64 Helicopter tail rotor drivetrain test stand for on-site data collection and analysis [1]. The test stand includes an AC input motor (Fig. 2(a)) rated at 400 horsepower to provide input drive to the configuration, a multi-shaft drive train supported by hanger bearings, flex couplings at shaft joining points, two gearboxes, and an absorption motor of matching rating to simulate the torque loads that would be applied by the tail rotor blades. The test stand, with picture provided in Figure 2(b), was used to collect data to be used in conjunction with historic helicopter vibration data to develop the baseline of operation for the systems under test. The signals are collected during the operational run of the apparatus included vibration data measured by accelerometers, temperature measured via thermocouples, and speed and torque measurements. The measurement devices were placed at the forward and aft hanger bearings and both gearboxes. This paper focuses on the application of time-frequency techniques to the forward and aft hanger bearing vibration signals denoted as S_1 and S_2 in Figures 2(a) and (b). The physical separation of between accelerometers (which will further be referred to more generally as sensors) on the bearings is 3.43 m.

3.3 Data Acquisition

The data acquisition software collects data from the hanger bearings once every two minutes during the course of the thirty minute baseline runs, with the exception of two additional collection periods at the start of the run, a total of 17 measurements. An experimental run consists of an intermediate speed ramp from 0 to 600 RPM followed by a ramp from 600 to 4863 RPM. The measurements for baseline characterization were then taken during operation of the test stand at a constant rotational speed of 4863 RPM from the prime mover with a simulation of output torque at 111 ft-lbs from the secondary. A summary of test conditions is given in Table 1 given a few conventions. Rotational speed is the speed of the input shafts and hanger bearings. Output torque is given by the torque at the output of the tail rotor gearbox simulating rotor operation while the torque applied to the input shafts and hanger bearings is equal to 32.35 ft-lbs.

Data collection yielded 65,536 point at a sampling rate of 48 kS/s per scheduled sampling period, which results in a data collection time of roughly 1.31 sec per acquisition. For each run, data was acquired 17 times on these 1.31 sec intervals: twice at the beginning and then once every two minutes until the end of the run. With individual data files containing 65,536 samples each, acquisition results in over one million data points per set,

Table 1: Loading profile for a 30 minute baseline test run

Rotational Speed (RPM)	Output Torque (ft-lb)	Input Torque (ft-lb)	Duration (min)
0-600	0	0	7.5
4863	111	32.35	30
600-0	0	0	7.5

which is too intensive for many processors to handle during time-frequency analysis. In order to resolve this computational issue and decrease computation time, each data set under test was divided into 17 experimental frames to correspond to each time the sensor was activated to collect data. Each of the 17 experiments was then divided into 16 windows comprised of 4096 points each. Within these subdivided windows, spectrogram measurements were made on both S_1 and S_2 while the mutual information measure was applied to 4096 point segments of S_1 and S_2.

Additional windows can determined by an overlap percentage which layers additional 4096 point windows within the main 16 in a given experimental frame at intervals of 4096 multiplied by the overlap percentage in order to create additional effective mutual information measurements from the given data. An overlap of 33 percent was determined to provide adequate clustering and enhance the probability density for implementation of predictive confidence levels.

This overlap selection helps eliminate data outliers and improve the visualization of the clustering when applying the time-frequency mutual information described in Section 2.7 to multiple data points. Therefore the total number of mutual information measure points for the given data is equal to the number of experimental frames (17) multiplied by the number of window signal subsets (16) and the inverse of the fractional overlap percentage (3), for a total of 816 mutual points or 272 mutual points when neglecting overlap components. The data format of the time series is also provided in [15].

The configuration of the test stand uses balanced drive-shafts aligned in a straight assembly as a baseline for normal operations. After performing test runs in the baseline condition, intentionally faulted configurations are tested to expand the baselines to include combinations of misaligned and unbalanced shafts. The goal of the time-frequency analysis is to establish metrics for the baseline conditions using the original data set and produce a set of metrics to diagnose each of unbalanced and misaligned conditions. The data presented for analysis included five sets of thirty minute runs of the apparatus each taken with different alignment and balancing conditions. Table 2 displays these conditions and their designations.

The primary physical fault conditions characterized experimentally are bearing unbalance and shaft misalignment. While these conditions will be described more thoroughly in Section 3.4, an overview of these settings helps in gaining a familiarity with the experimental set up. The nomenclature of the baseline sets is dictated by numbered segments of the drive-train. Each segment of concern in experimentation is designated by a number (1 through 5) and coupled by flex couplings at the bearings locations to hanger bearings. Unbalance is related to drive shafts which exhibit geometrical or mass centerlines that do not coincide with axes of shaft rotation (UB/A and UB/MA cases). These will be referred to as the unbalanced-aligned (UB/A) and unbalanced-misaligned (UB/MA) cases respectively. Misalignment (MA/B, UB/A and MA/UB cases) in the test configuration is characterized by a change in bearing and shaft placement that moves the number 3, 4, and 5 shafts from straight alignment to produce an angle of 1.3 degrees. Either a 3-5 unbalance (unbalance of three consecutive drive shafts) or a 4-5 unbalance (unbalance of only two drive shafts) differentiates two experimental settings. The aforementioned settings will be referred to as the misaligned-balanced (MA/B) and unbalanced-misaligned (UB/MA) 3-5 and 4-5 cases. These settings produce additional wear on drive-train components while also presenting additional transients in harmonics that can be measured for health classification purposes. For the purposes of this paper we will simply refer to these cases as baseline (A/B), misaligned (MA/B), unbalanced (UB/A), and misaligned-unbalanced (MA/UB) as shown in the nomenclature of Table 2. Instances of ambiguity between the misaligned-unbalanced cases will be specified as 3-5 misaligned or 4-5 misaligned.

Table 2: Tail Rotor Driveshaft Experimental Settings

Shaft Status	Balanced	Unbalanced
Aligned	A/B	UB/A
Misaligned	MA/B	MA/UB 3-5, 4-5

Unbalance vibrations are generated when geometrical centerline or mass centerline of a shaft do not coincide with the rotational axis of the shaft, for example in cases of bearing looseness or due to manufacturing imperfections. This inconsistency between rotational axis and geometrical or mass centerline creates a radial bow force F_u at a fixed relative phase angle, φ, which varies in magnitude along the length of the shaft as shown in Figure 3-(b). The unbalance condition creates harmonically varying vibrations, D, on a hanger bearing housing, which are registered by dedicated accelerometers. These varying vibrations consist of x and y axis radial vibrations, z axis axial vibrations, and torsional vibrations of a shaft in a bearing (Figure 3-(b)) as well as additional vibration signal contributions coming from coupled bearings, gearboxes, power units, airframe, and other components. Each hanger bearing on a helicopter system has only one dedicated accelerometer in current settings, which can pick only lateral x axis component of the vibrations (Figure 3-(c)) of the form:

$$D_x = A_x \cdot \cos(\omega t + \psi_x) \tag{52}$$

$$D_y = A_y \cdot \sin(\omega t + \psi_y) \tag{53}$$

where $D_{x,y}$ and $A_{x,y}$ are displacements and amplitude of displacements in x and y axis directions, ω - angular velocity, and $\psi_{x,y}$ - phase angles.

Vibrations caused by unbalance will be in-phase on both bearings accelerometers S_1 and S_2 when $(\varphi_y - \varphi_x = 0)$, and will vary only in magnitude depending on the magnitude of unbalance, F_u. The drive shaft supported by the hanger bearings at sensor locations S_1 and S_2 is not a uniform shaft but rather a sectionalized shaft as previously described. Therefore, misalignment cannot typically be avoided. It should be noted that as shown in Table 1 the experimental data is gathered under conditions of constant or near constant torque load and speed.

Misalignment in our case is considered as an angular misalignment when the shaft centerlines of the two shafts meet at angle with each other. This, on the contrary to unbalance, causes axial preloads on the shaft in the z axis direction, and can be decomposed to x signal component based on angle of misalignment $F_x = F_z sin(\alpha_m)$. This force will have the greatest impact on the bearing closest to the shafts' coupling point, and will have a phase difference in reference to force registered at a further located sensor $(\varphi_y - \varphi_x \neq 0)$ (Figure 3-(c)) because of finite stiffness and dampening in the system. In industrial vibration monitoring one would use shaft diagnosis techniques such as shaft centerline orbit monitoring, which requires two x and y sensors at a single location, and a skilled human operator, which make such technique inapplicable in our case and justifies the need for an advanced diagnostic measure. Mutual information measure takes advantage of two accelerometer

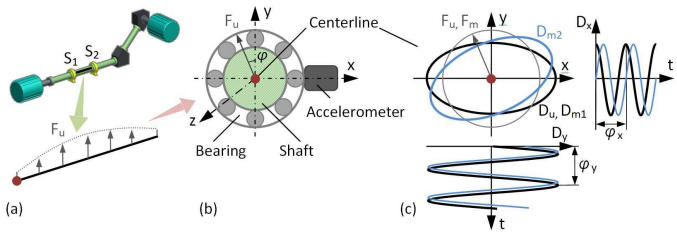

Figure 3: Unbalance force distribution over the shaft supported at the S_1 and S_2 accelerometers locations (a) cross-section of a bearing and the shaft at the S_1 accelerometer location (b) shaft centerline orbits at the S_1 and S_2 accelerometer locations, and (c) displacement or vibration components in the x and y axis directions (D_u, D_{m1} orbits when $\varphi_y - \varphi_x = 90^\circ$, D_{m1} when $\varphi_y - \varphi_x = 120^\circ$)

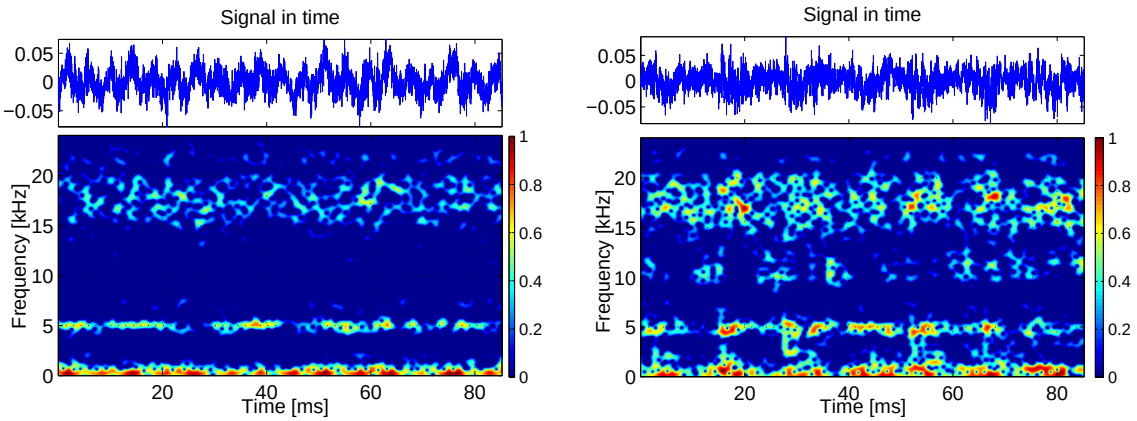

(a) S_1 of baseline

(b) S_1 of MA/UB 3-5

Figure 4: Spectrogram of S_1 for (a) baseline (B/A), and (b) misaligned-unbalanced (MA/UB 3-5).

signals located at different locations, simultaneously quantifying all frequency and phase components of the mechanical vibrations signals.

3.4 Vibration Analysis

In the predictive maintenance practices of CBM, metrics similar to the simpler total harmonic distortion (THD) or root mean squared (RMS) classical methods are used as diagnostics. These provide comparisons of a signal harmonic component (such as the fundamental) to other harmonics in weighted algorithms. These metrics provide good indications of vibration characteristics under the condition that the frequency components under test are stationary, or remain unchanged with the progression of time.

Unfortunately, this classical approach inherently assumes the disturbance is of a periodic nature. In fact, not all real life disturbance events result in periodic waveforms and transient frequency variations are common in the event of faulted components. Often events such as damage cause disturbances that can best be characterized as transient in nature. In such cases it is necessary to study the time-varying frequency components of a disturbance. This can be accomplished with time-frequency analysis.

The motivation to use time-frequency analysis is to have the ability to represent and analyze non-stationary signals whose spectral characteristics change in time. One approach to time-frequency analysis is to take the time-frequency distribution of a signal.

The problem with WV distribution is that it introduces artifact when a signal is multicomponent between existing components (on auto terms) at non-linear spacings (cross-frequencies). This artifact can be reduced with CW, RID, and ZAM distributions, shown in Figure 5(a)-(f). The ZAM kernel was selected for this project for its its general capability to represent a fair tradeoff in time and frequency resolution. The window for this function is selected based on the number of frequency bins (N = 1024) with the Hamming window being selected in both time and frequency smoothing. The time and frequency window lengths are given as N/10 (or 103) and N/4 (or 255) respectively with rounding to the nearest odd number. Looking at the time-frequency distributions of the two signals, we can see that the first signal (advanced state) has four frequency bands while the second signal (damaged state) has two frequency components with increased energy in the second harmonics and decreased energy in the first harmonics. However, the second signal seems to have more transient variation among the frequency bands. We will search for a way to define this transient variation. The metric $H_\alpha(C_s)$ defined in (40) measures the number of signal elements of $s(t)$ over the time and frequency planes.

Figure 7 is a metric derived from the Rényi information of the time-frequency distribution. In Figure 7(a), the Rényi information or entropy of the of Wigner-Ville kernel is compared to that of the reduced interference distributions. From the metric, we can see a higher value for the amount of information as represented by the

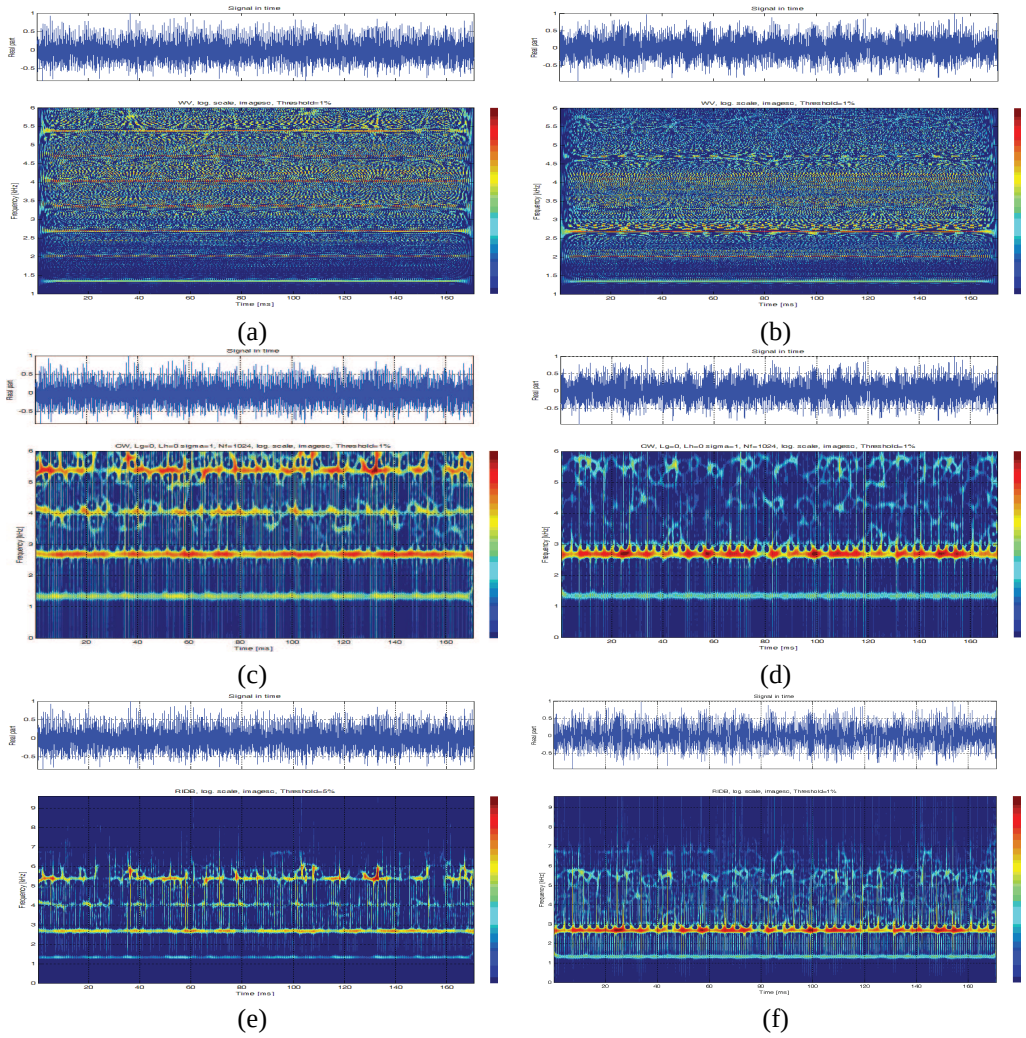

Figure 5: Time-frequency distributions of vibration signals from (a) data set 1, and (b) data set 2 with WV distribution, illustrating the potentially negative impact of cross terms in vibration analysis.

reduced interference distribution. This can be interpreted similarly to visual inspection of the time-frequency distributions for the respective kernels. By visual inspection of the reduced interference distributions, we see more of the information represented in the transient variations of the signals and less of the cross-terms. The values of these test points (1-10) are randomized within the week long duration of testing approaching failure in our case study, so we will now view the sorted version of the same data and consider the metric for a sequential interpretation approaching failure. This will help us view the Rényi information as a metric for condition assessment.

The sequential time-series to failure is shown in Figure 7(b). The bars corresponding to 1, 2, and 4 showcase approximately the same complexity by our metric and all correspond to the start of an experiment run. However, bar number 7 corresponding similarly to the start of an experimental run, shows a significantly higher complexity value while actually decreasing in the number of frequency bands (as seen from Figures 4-6). This corresponds to high amount of frequency transient information caused by the impending failure. Extensive damage was likely caused during the previous runs at the values indicated by high Rényi metric and failure occurred soon after the measurement used for bar 10. Constant increase is seen from bar 3 to 5 to 6 leading up to failure, and it will be interesting in the future to consider sections that have been completely matched in terms of the

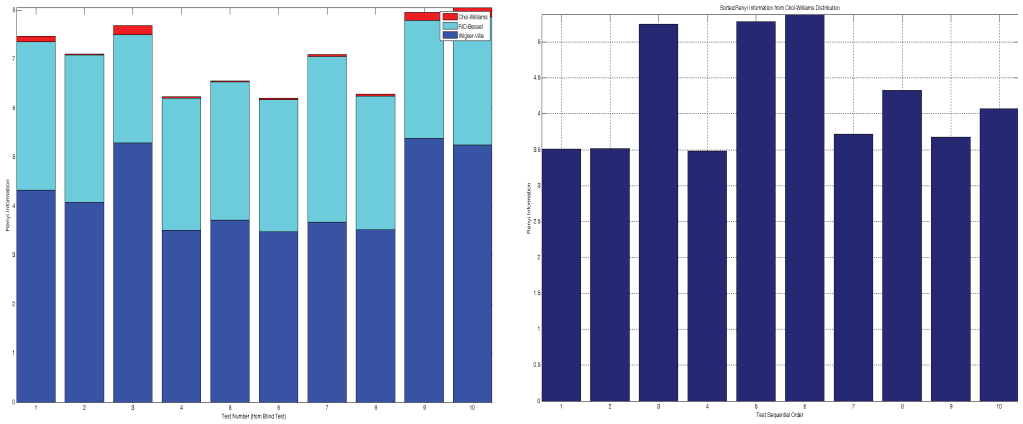

(a) (b)

Figure 6: (a) Rényi metric comparison, and (b) sequential sorting of metric for the CW.

test sequence (both loading and rotational speed). With the given results, we would suggest using the Rényi metric derived previously to confirm that a part is failing. If the second harmonic of the gear mesh frequency measured here were increasing, we could measure the Rényi based metric and confirm that while the number of frequency bands from 1x of mesh to 4x of mesh frequency is decreasing, the Rényi information is increasing. This would indicate a high number of transient variations and allow for rejection of some false positives based on the previous metrics of first and second harmonics of gear mesh frequency.

3.5 Comparison of Rényi Derived Self Information to Time-Frequency Methods

The first step of analysis and discussion uses the self Rényi information measure defined in (40) of Section 2 to describe the individual time series. The self Rényi information measures of S_1 and S_2 for baseline and misaligned cases are provided in Figure 7. Signal 1, S_1, and Signal 2, S_2, in both the baseline (A/B) and misaligned (MA/B) cases are processed by applying the 8-point moving average filtering followed by Rényi information calculation to obtain the self information measure. Thus, for every time instance of every experiment window of the data, a Rényi calculation of each auto-correlated signal was gathered. As shown in Figure 7, a total of 272 self information measures were gathered for each signal of each case. Additional overlapping is used for x-y coordinate mapping used in visualizing part health. In order to identify the tendency of the measure, an 8-point moving average filter was applied to each signal with the filter covering half of the time instances provided in each experiment window. The results of this self information measure are compared side by side in Figure 7 for each signal. The referenced time instance (15th of file frame at 5th experiment window) is marked on each graph to show a consist reference point based on the description of Section 2.

Notable difference from the side by side comparison in Figure 7 is a sizable increase in the self information measure of the misaligned case over the baseline case. This could be a characteristic signature of a misaligned case. The self information measure shows a general increase at the given samples when comparing the balanced-aligned case with the misaligned case and an increase on the average of measured frames. The average self information value of the baseline S_1 signal is reported at 6.72 bits while the average value of the same signal in the misaligned-balanced case was 7.68 bits. Comparing the second signal set, S_2, we obtain a value of 6.78 bits compared to 7.31 bits for the same cases. However, from this derived metric, the interpretation is yet unclear. This self-information measure can be verified using the spectrogram example discussion in Figure 4. From this data, there is little other indication of change from the baseline case to another "faulty" status of the shaft. Moreover, the self Rényi information of S_1 in the balanced case in Figure 7(a), as well as both signals in the misaligned case, oscillate more compared to the self Rényi information of S_2 of the baseline case (A/B). This could be attributed to more high frequency components shown in the time-frequency spectrogram of Figure 4(b).

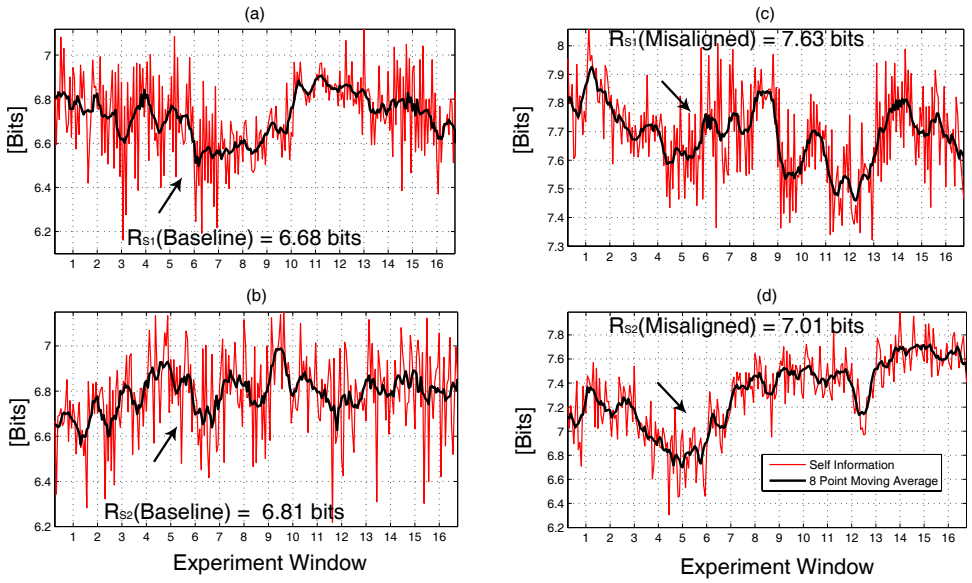

Figure 7: Self Rényi information measure of S_1 and S_2 for baseline in (a)∼(b), and self Rényi information measure of S_1 and S_2 for misalignment in (c)∼(d)

While this self information proves useful and shows a notable basis by which to compare data sets, it lacks potential for comparison of closely related signals and in this instance shows an increase when compared on average while not for localized comparison. This only partly supports the desired qualities of a condition indicator while further information can be gathered from the mutual information measure. This mutual information measure is a complex value and can be further subdivided into two constituent values: an in-phase mutual time-frequency information ($I_\alpha(R_{s_1s_2})$) and a quadrature mutual time-frequency information ($I_\alpha(Q_{s_1s_2})$) defined in (48) and (49).

3.6 In-Phase and Quadrature Components of the Time-Frequency Mutual Information Measure

Mutual information measures of baseline and misaligned cases are provided in Figure 8. An interesting trend can be seen in the baseline case in Figure 8(a). Overall, the in-phase mutual time-frequency information ($I_\alpha(R_{s_1s_2})$) stays mostly at a constant separation from the quadrature mutual time-frequency information ($I_\alpha(Q_{s_1s_2})$). Both the $I_\alpha(R_{s_1s_2})$ and $I_\alpha(Q_{s_1s_2})$ of the baseline case in Figure 8(a) remain relatively constant throughout all windows of the experiment. However, toward the end of the sequence outlined in Figure 8(a), the in-phase and quadrature mutual information measure values begin to experience a larger separation. These characteristics are all important to note while considering what truly characterizes the baseline physics of the system.

A glance at the mutual information from the misaligned case in Figure 8 (b) draws attention to two distinctive signatures. First, like the baseline case, the co-spectral mutual time-frequency information ($I_\alpha(R_{s_1s_2})$) remains relatively constant throughout all experiment windows with a large trough around experiment window 10 corresponding to a minimum value of the quad-spectral mutual time-frequency information ($I_\alpha(Q_{s_1s_2})$). Second, the quadrature component has a larger average value over the length of the experiments than was seen in the quad-spectral component in the baseline case. Also, the quad-spectral component in the misaligned case fluctuates greatly, showing greater amounts of local minima and maxima. Though the quad-spectral information in the misaligned case revealed a significant rise in the number of bits in the mutual information measure, the co-spectral portion showed little increase over the experiment windows measure. By comparing the results in Figure 8 with other results by classical spectral analysis or traditional spectrogram, one can find the useful-

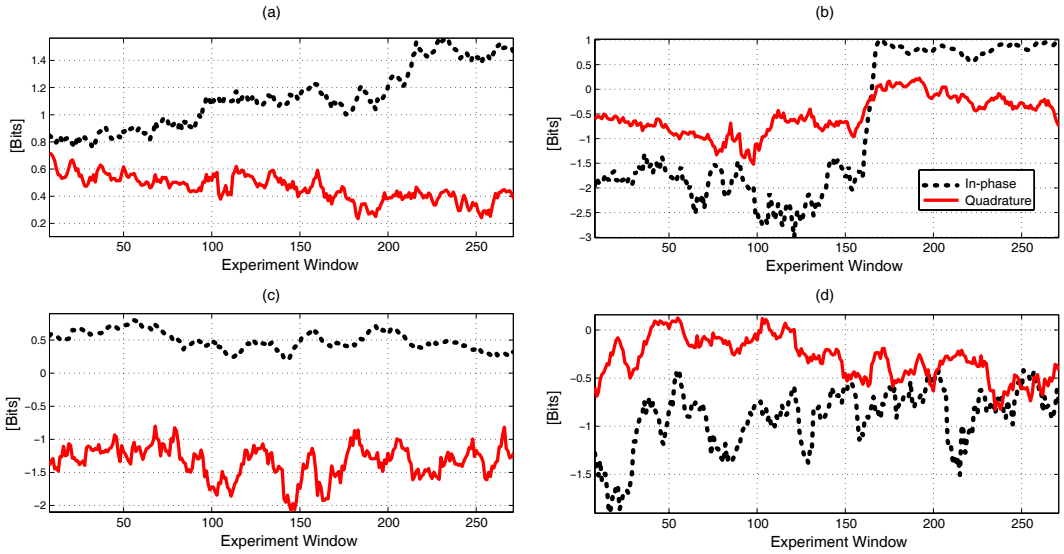

Figure 8: Mutual Rényi information measure of S_1 and S_2 for (a) Baseline-Aligned, (b) Aligned-Unbalanced, (c) Misaligned-Balanced, and (d) Misaligned-Unbalanced

ness of the proposed technique for a quantitative health condition assessment of the experimental setup. Further analysis is underway to understand the relationship between the time-frequency mutual information method and other confounding factors such as speed and torque, isolating the sources of transient changes in the vibration signatures.

3.7 Time-Frequency Mutual Information Measure Visualization

The mutual information measure currently in development and shown in Figure 9 provides a graphical interpretation of part condition by analyzing the amount of mutual data shared between two vibration signals received from separate accelerometers. The mutual information measure is comprised of a quadrature component and an in phase component which, by observation seem to indicate differences in the actual physics of the system. Figure 9 shows the scatter plot distribution of the in phase component of the measure on the x-axis and the quadrature component of the measure on the y-axis. In the condition of system unbalance, as seen in Figure 9 (a), (c), and (d), which compare misaligned and unbalanced experimental settings to the standard baseline, the in-phase component shows a potential trend toward a decrease in information bits.

Similarly, misalignment can be observed to decrease the number of information bits of the measure contained in the quadrature component, provided in Figure 9 (b) and (d). As a distribution these values can be seen to shift along the x-y plane indicating a shift in part or system status. Additional studies should be analyzed and compared to determine if these trends are truly linear as they appear to be from observation. It would appear that Figure 9 (c) and (d) which were tested under both misalignment and unbalance conditions, as well as combination settings, have differing degrees of misalignment and unbalance yielding different distributions which follow the established trends along the quadrature and in phase components.

4 Health Monitoring of Electric Cable

4.1 Introduction

In order to prevent electrical outages and to save maintenance expenses, a prognostic technique is needed which can quantify the degradation of the insulation of a cable to predict the remaining life of the cable. Ideally,

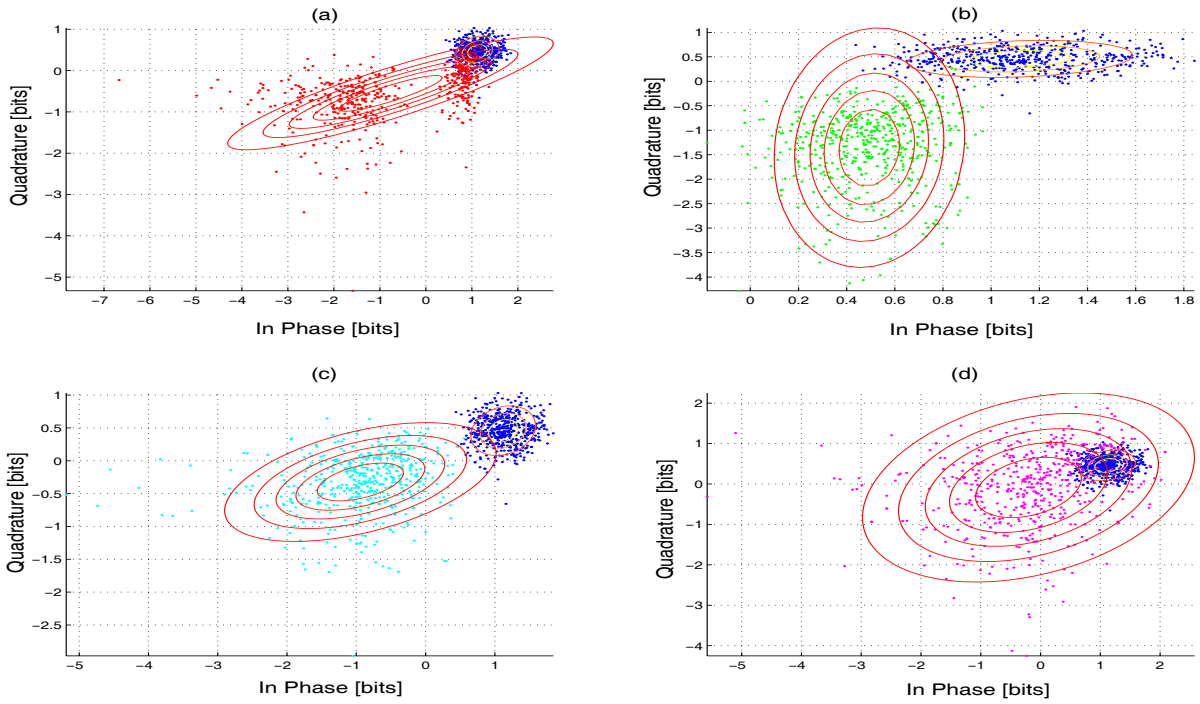

Figure 9: Baseline comparisons of the mutual information measure (a) Aligned-Unbalanced, (b) Misaligned-Balanced, (c) Misaligned-Unbalanced 3-5, and (d) Misaligned-Unbalanced 4-5 with the Aligned-Balanced Case

the technique should be non-destructive, non-intrusive, applicable to cable types and insulation materials commonly used. Furthermore, the ideal scenario is to be able to accurately monitor the health status of cable in real-time and continuously. Recently, the NRC and Brookhaven National Laboratory have been working on the diagnostics and prognostics of electric cables with the Broadband Impedance Spectroscopy (BIS) technique developed by Boeing [31]. On an international scale, the OECD Halden Reactor Project in Norway is researching similar issues in monitoring the condition of electric cables; their method is known as Line Resonance Analysis (LIRA) [32]. The purpose of these techniques is to detect and locate defects before they cause a component to fail. Although BIS and LIRA have different names, these two methods both monitor impedance of faults caused by insulation degradation using frequency-domain reflectometry (FDR), primarily due to the extreme challenges involved in accurately measuring fault impedance in the time domain.

In practice however, there are no condition monitoring techniques available that have all the above attributes. The capability of joint time-frequency domain reflectometry (JTFDR) to monitor the status of cable insulation is evaluated in an effort to predict the remaining life of power cables. JTFDR captures the advantages of both TDR and FDR while avoiding some of their limitations by using advanced digital signal processing [30]. A distinct advantage of this reference signal is its configurability; the user can select appropriate parameters of the reference signal, including frequency bandwidth, center frequency, and time duration, by considering the frequency characteristics of the wire being tested. JTFDR has been proven to be able to accurately and sensitively detect both hard and incipient defects on coaxial cables [31]. The unique features of the time-frequency cross-correlation function employed by JTFDR also allow it to monitor the minor changes in cable insulation which indicate the health status of the cable with a high degree of sensitivity.

4.2 Experimental Setup

Shown in Figure 10(b) is the system function diagram that describes the configuration and function of the experimental devices of the JTFDR wiring test bed. The computer (PC) instructs the arbitrary waveform generator

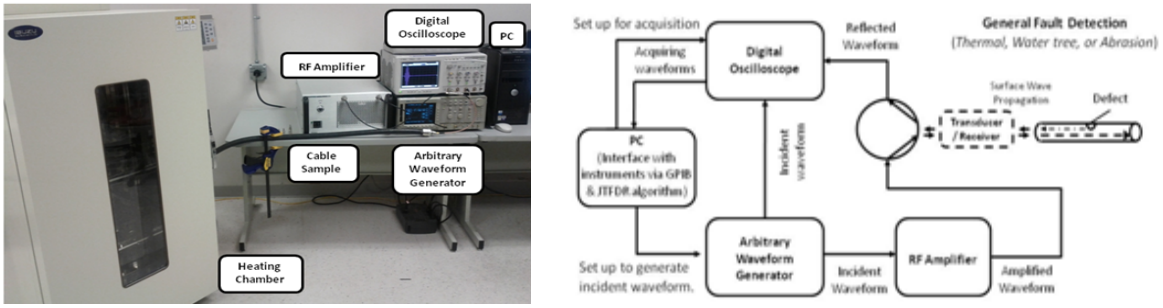

(a) (b)

Figure 10: Experimental setup is shown with a (a) labeled figure of the laboratory setup and (b) a system function diagram

to produce the Gaussian-chirp incident signal designed based upon the input center frequency, bandwidth, and time duration with optional variations in reference signal described such as sinusoidal modulation. This incident signal propagates into the target cable via the RF amplifier in cases of longer cable lengths, is reflected at the fault location, and travels back to the signal launcher/receiver. The signal launcher/receiver should be seen as a general implementation with a circulator or switch being used for this task in laboratory settings while future work would implement a wireless sensor for insulation assessment. The reflected signal is redirected to the digital oscilloscope. The computer program acquires both the incident and reflected signals from the oscilloscope, calculates the time-frequency distribution of the incident and reflected signals, and executes the time-frequency cross-correlation algorithm to detect, locate, and assess any defects on the cable. The heat chamber used for accelerated thermal aging is also shown in Figure 10(a). For longer or more dispersive cable media, we make use of an RF amplifier (120W ouput) to provide increased range of detection while keeping a l meter or better resolution for the JTFDR method. This helps stabilize against instrumentation noise for the AWG and oscilloscope while also providing sufficient resolution for detection multiple reflections of the incident reference signal.

4.3 Diagnostics and Prognostics

4.3.1 The Modified Arrhenius Equation

Typically aging of a cable is defined as any process electrical, mechanical, thermal, or environmental which might reduce the overall effectiveness of the cable for power or signal transmission. An alternative, and broader, definition of aging would describe the process as any condition over the duration of cable life that leads to increased susceptibility to hardware faults or that might otherwise lead to premature failure. In our case, actual aging is represented broadly by a simulation of thermal stress and in particular by uniform heating of a section of cable at a constant temperature above the normal thermal capacity. As defined by IEEE 1064 standard, aging is the occurrence of irreversible deleterious changes that critically affect performance and shorten useful life [27].

The well known Arrhenius model is used to determine the aging test parameters such as thermal stress and time duration. The Arrhenius model is based on chemical rate theory and has been verified to be effective for many solid materials. The equation of the Arrhenius model describes the relationship between the reaction rate and the temperature of a chemical reaction [13]. One key point to remember is that this reaction rate and temperature correlation only applies to a single reaction, while insulation degradation is not a single chemical process, but rather more complicated with multiple reactions and often nonlinear deleterious effects. This model has however become accepted as an indicator and metric for cable aging as outlined in the IEEE standard. The modified Arrhenius equation for an accelerated aging test follows:

$$\frac{t_s}{t_a} = e^{[E_a/B(1/T_s - 1/T_a)]} \tag{54}$$

where the following hold true:

T_s is the service temperature;
T_a is the accelerated aging temperature;
t_s is the aging time at service temperature;
t_a is the aging time at acceleration temperature;
E_a is the activation energy of the material;
B is the Boltzmann's constant (given below),

$$B = 8.617 \times 10^{-5}[eV/K] \tag{55}$$

This equation equates the heating of a material at temperature T_a for time t_a to the aging of the material at the service temperature T_s over a time t_s.

4.3.2 Accelerated Aging Test with Various Low Voltage Insulation Types

Using the previously described modified Arrhenius equation as a guide for accelerated aging, and utilizing standard activation energy values for various cable types, tests were performed on low voltage control and instrumentation cable to simulate 120 years of service life at 50 degrees Celsius, nearly double the expected service life of a typical cable. During the accelerated aging tests, JTFDR is employed to assess the various states of the cables during the aging process and growth in measured time-frequency cross correlation peak value growth. Before any external thermal stresses are applied, the waveforms are acquired multiple times to account for noise and acquisition error and processed for each cable sample to obtain the time-frequency cross-correlation baselines for future comparison. Only a localized segment (typically 1 m) is aged to simulate non-uniform aging along the length of a cable sample (10-20m for verifying tests). A certain number of hours (t_a), is computed depending on how long, (t_s), the cable is to be aged. When the cables are to be measured using the time-frequency cross correlation metric at regular intervals, the "hot spot," or aged segment, is cooled to ambient temperature to ensure that all metric increases are related to actual simulated aging and not simple geometry changes within the cable samples. The waveforms are acquired and processed after this cooling process is verified with a thermometer to obtain an updated time-frequency cross-correlation plot. The program then calculates the peak value corresponding to the aged segment and records this new value for comparison with previously collected and future health assessments.

4.3.3 Accelerated Aging Test with Medium-High Voltage Cable

In the case of XLPE cable, an activation energy E_a of 1.33 eV [15] was used with an acceleration temperature of 140°C. The typical maximum operating temperature of MV-90 cable is 90°C. With a an acceleration temperature of 140°C and a simulated service temperature (T_s) of 90°C over 90 years (t_s), the simulated aging time can be found to be 24 hours.

Aging was simulated using a heating chamber with two through ports for cable access separated by 0.6 meters. A meter long "hot spot" was desired for localized aging, however, in the case of thicker MV-90 underground cable, minimum bend radius along with cable stiffness and thickness allowed only 0.6 meters, or the separation between cable through ports, for hot spot consideration. Both XLPE insulated cable samples (Rockbestos Firewall III XHHW, low voltage and MV-90, medium voltage) were heated for one hour at a time at 140°C. The cables were then cooled to ambient temperature (25-27°C) as measured by an infrared surface thermometer before measurement. Cooling time, varying from 40 to 50 minutes, was allowed to prevent results from being obfuscated by other potential sources of reflectometry variation such as geometric changes of insulation and conductor materials.

Measurements were taken using an 8 GSa/s digital oscilloscope to record the raw data of each acquisition of sampled signals (incident and reflected) along with the initial reference signal. These signals were then evaluated using the JTFDR method.

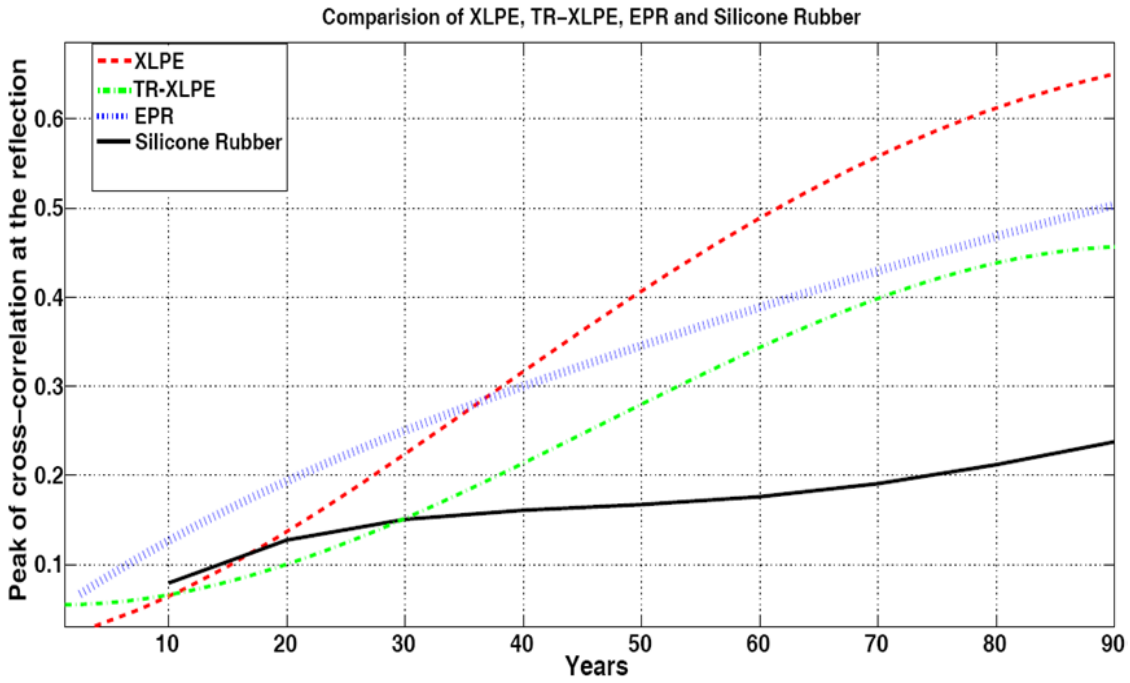

Figure 11: Comparisons of low voltage cables with cross-linked polyethylene (XLPE), ethylene propylene rubber (EPR), and silicone rubber (SIR) insulation types to tree-resistant medium voltage cable (TR-XLPE)

5 Conclusions From Completed Work

In this project, two sets of vibration signals have been analyzed with four different kernels - WV, CW, RID, and ZAM distributions. For these vibration signal analyses in time-frequency domain, WV shows some cross terms which are reduced with CW, RIDB, and ZAM distributions. We have shown which frequency components are responsible for the vibration introduced by the mechanical components in the test bed system as well. In addition to this, comparison of time-frequency distributions it is possible to identify which component is in an advanced stage and which component is potentially damaged. Moreover, from Rényi information it can be concluded which time-frequency distribution provides more information for the vibration signal analysis. Based on all the analyses provided in this project, necessary steps can be taken for health improvement of components in order to avoid premature failure.

Drawing from Rényi complexity measures and mutual information theory, baseline, unbalanced, and misaligned experimental settings are quantitatively distinguished by the proposed mutual information technique. Statistical analysis of the time-frequency information measure from Table 3shows a variance in the proposed in-phase and quadrature information measures of 0.0070 (STD of 0.0837) and 0.0054 (STD of 0.2324) respectively for baseline testbed conditions in opposition to an increased in-phase information measure variance of 3.33 (STD of 1.8258) in repeated unbalanced test cases and increased quadrature information measure of 1.7497 (STD of 1.3228) in repeated misaligned cases. With unbalance quantifiable by variance in the in-phase mutual information and misalignment quantifiable by variance in the quadrature mutual information, machine health classification can be accomplished using statistical bounding regions. In summary, the baseline can be characterized with a constant separation on a per-time instance basis of the mutual information measure. The misaligned case may be characterized by its quadrature component. This component shows the misalignment in a relatively large, increased number of bits from the information measure. However, similarity still remains in the in phase component whether the case is aligned or misaligned.

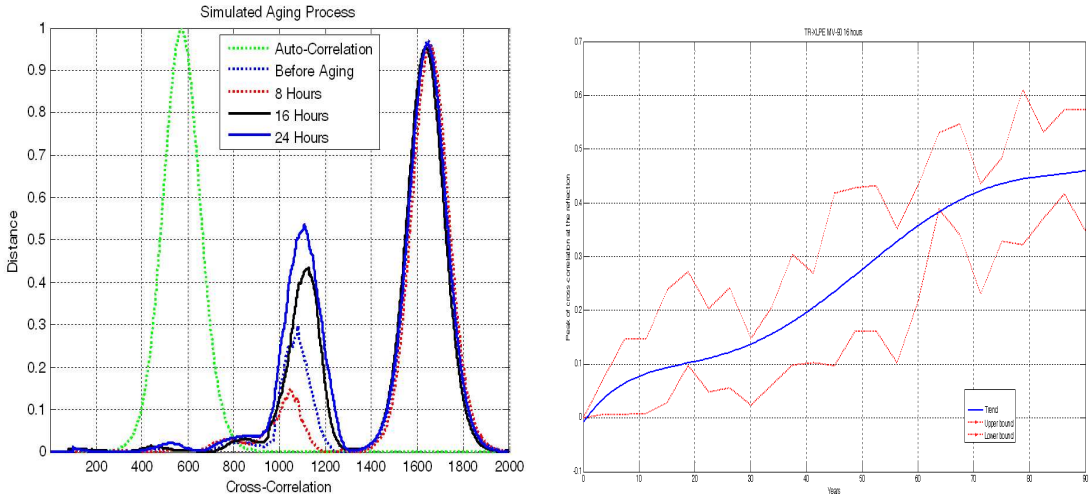

(a) (b)

Figure 12: Medium voltage MV-90 cable time-frequency cross correlation peak growth index growth shown by (a) cross correlation peak curves at progressive aging values and (b) summary of peak growth over time

6 Proposed Work

6.1 Mutual Information Based Condition Indicator for Drivetain Health Monitoring

Included in Table 3 is reference for the statistics related to both spectra of the mutual information measure proposed. Future studies of this indicator method could focus on varying states of misalignment and unbalance to determine a quantifiable relation between the x-y distribution shift and part health. Differences in this mutual information measure could be further developed into an increased precision statistical indicator of part or system health status.

This metric could be used in the fusion of other types of sensors in order to obtain extended information for more accurate assessment of the health status of components. Data could be gathered from vibration, acoustic, and temperature sensors and correlated to present a single, more robust, health indicator [28], [29]. Furthermore, analysis of these values can yield great insights into the physics behind systems such as the system under study which provided the mechanical vibration data, providing either a simple summary of component health for an operator or a complex interpretation from a knowledgeable engineer in order to fully achieve condition-based maintenance. I have been seeking access to the Integrated Maintenance Data System (IMDS) through contacts with the South Carolina Air National Guard for historical data from Apache aircraft and aim to provide historical parameters and integrated statistical bounds to my Mutual Information Measure metric.

Table 3: Statistical Summary of Mutual Information Measure

Statistical Parameter		Baseline	Aligned-Unbalanced	Misaligned-Balanced	Misaligned-Unbalanced 3-5	Misaligned-Unbalanced 4-5
Mean μ	*In Phase*	1.1202	-0.7424	0.4902	-0.9535	-0.1753
	Quad	0.4535	-0.5509	-1.3691	-0.3268	-0.0726
STD σ	*In Phase*	0.0837	1.8258	0.2147	1.0136	1.4344
	Quad	0.2324	0.7107	1.3228	0.4852	1.2363
Correlation ρ		0.2326	0.8732	0.0891	0.4005	0.3188

6.2 Comparative Study of Aged Segments by Joint Time-Frequency Domain Reflectometry

This section will serve as a method to introduce new proposed research pertaining to low voltage or instrumentation and control cable health assessment. This topic has already been addressed to some degree in the previous research, however, a number of advances could be made to aid in making JTFDR a feasible and practical method of either continuous or periodic monitoring of cable systems. Key problems with the current methodology for this subset of reflectometry are (1) the direct electrical connection that requires removal of tested cable samples from service and additional labor, (2) additional time and effort for determining the proper optimal reference for a given cable sample, (3) the ideal conditions of the laboratory which do not account for common operating conditions of generation facilities and industrial centers, and (4) the accelerated aging process for cable health tests which can be seen as somewhat preliminary in status. As a means of addressing these points, first discussion will be presented for an alternate means of injecting a reflectometry signal for insulation health assessment by surface wave. An optimal reference has been developed for such conditions and will be further developed in proposed work. Next, an automatic algorithm will be proposed to find the best reference signal for JTFDR based on weighted factors such as size of time-frequency cross correlation peaks. Also, improvements to the laboratory experimental design will be suggested to take into account potentially confounding factors and more realistic aging. The ultimate goal of these updates would be to promote progress for areas of research in smart grid or networked power systems where a non-invasive in-situ monitoring device for cable would be of great benefit.

6.2.1 Implementation of Time-Frequency Domain Reference in Dispersive Environments

In order to counter the dispersion properties of the antennae based surface wave signal injection methods, a secondary sinusoidal modulation is explored relative to the existing reference signal that can further tune the optimal reference to a given set of narrowband slices within a larger bandwidth. A numerical simulation will now be derived to explain concepts of the surface wave optimal reference signal. In this simulation, two different impedance zones exist: a characteristic impedance region (before and after fault) and a faulted region represented by a change in impedance. This simulation was performed in MATLAB to emulate a 10 m cable with a fault at 6 m along the simulated sample. Figure 13(b) shows the surface wave optimal reference (topmost graph) injected into a cable with subsequent reflections at a fault segment at 6 meters and at the cable open end at 10 meters (middle graph). The time-frequency cross correlation algorithm (bottom) then compares the incident and reflected signals. The JTFDR metric is obtained from the peak of these cross-correlation values and will further be evaluated with experimental verification before addition work is proposed.

6.2.2 Implementation of Cable Health Assessment by Surface Wave Injection

Shown in Fig. 13(a) is the system function diagram that describes the configuration and function of the experimental devices of the JTFDR wiring test bed for non-invasive surface wave injection methods. The signal is then reflected at the fault location, and travels back to the signal launcher/receiver. A prototype surface wave launcher/transducer pair (pictured in Fig. 13)(a) was placed at each end of a 7 ft (2.1336m) cable sample and coupled to the cable using a concentrically wrapped length of conductive tape. This conductive tape was connected to the signal connector of the coaxial input by a thin filament and separated from the input coaxial return by a polystyrene spacer. The coaxial return was in turn connected to the ground plane. Initial tests were performed to evaluate the utility of the surface wave signal in OEM unshielded cable samples (600V low voltage, LSTSGU-9, SIR insulated) and a shielded sample (15kV medium voltage, TR-XLPE insulated cable).

The first step of practical implementation of surface wave reflectometry for non-invasive diagnostic coupling is detection of an open end. Further work must be accomplished to fully characterize the frequency response and dispersion characteristics of the broadband monopole surface wave launcher before implementation of the methodology described previously, therefore, these tests utilize a JTFDR reference signal of a chirp signal in time-localized Gaussian envelope. The Gaussian chirp signal used in these tests has a center frequency at 350 MHz over a 100 MHz bandwidth for a 0.9 s time duration.

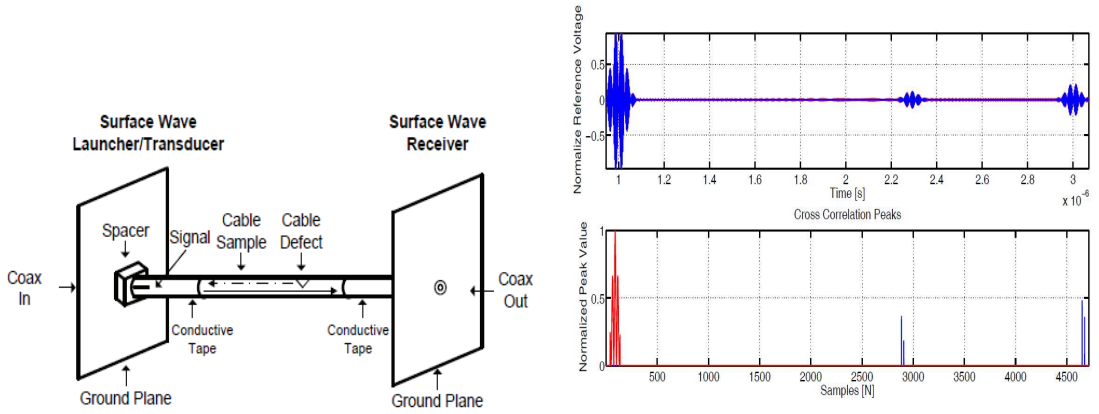

(a) (b)

Figure 13: (a) Experimental setup for Surface Wave Optimized and (b)Simulated defect on 10m segment of cable using the surface wave optimized reference shown in time domain (top)and by comparison using JTFDR (bottom).

Using the surface wave injection configuration of Fig. 13(a), we tested the unshielded, low voltage and shielded, medium voltage cable samples using the JTFDR algorithm and the results are shown in 14a and 14b for 2 meter segments of each cable type. In each figure, the autocorrelation peak of the reference signal is represented by the peak with the most energy, which displays the start of the cable or reference point of the incident signal. A time-frequency cross-correlation of the reference and reflected signals is then shown by further corresponding peaks with the difference between the two peaks (reference and first reflection), scaled by the propagation velocity and signal lengths, providing an estimate of the length of the cable.

By use of the described metric for the LSTSGU-9 SIR cable an estimated cable length to open circuit fault was described as 1.9822 m, a 7.1 percent difference from the actual length of 2.1336 m. Similarly for the MV-90 TR-XPLE cable, a length to open circuit fault of 2.2489 m was estimated by optimized surface wave, a 5.4037 percent difference from the same length. These results show promise for a potential fault location algorithm and further tests in proposed work will explore the adjustments to JTFDR metrics while testing longer lengths of cable.

6.2.3 Improvements of Experimental Set-up

Having recently begun collaboration with the International Atomic Energy Agency (IAEA), improvements to the testing setup at the University of South Carolina are in order before receiving additional cable samples from participants in the combined research project. As such, the first step in applying JTFDR is optimizing the reference signal used in reflectometry for the given cable. This is done by first performing a frequency sweep with a network analyzer or similar measurement configuration and then running a loop through time duration, bandwidth, and center frequency properties of the optimal reference to obtain the raw data and cross correlation peak data for a range of references. From there, an operator must parse through a table of values collected from the looping operation and visual inspection of waveforms to determine a proper selection.

A proposed task for improvement of this process is to base optimal reference selection around key parameters identified by visual inspection to provide a good indication of spatial resolution in fault location and sensitivity to changes in the metric. Parameters to optimize the reference include the width of peak pulses, where shorter width typically indicates better spatial resolution. Additionally, minimal noise between peaks and a higher number of reflections along with a higher sweeping frequency typically indicate better accuracy in measurement. From these factors, an algorithm can then be derived along with optimizing equations relating the bandwidth and sweeping frequency of the reference signal.

In seeking guidance from sponsors in both the Nuclear Regulatory Commission (NRC) and IAEA, further

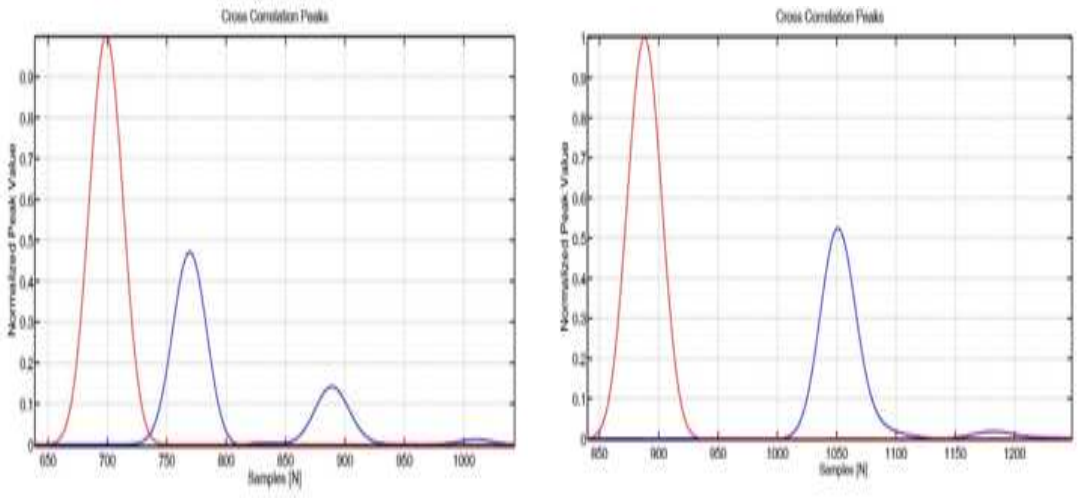

(a) (b)

Figure 14: Time-frequency cross correlation metric for open end measurement on 2 meter segment of (a) cable in low voltage unshielded case and (b) cable in medium voltage shielded case with stripped injection point.

experimental upgrades have become apparent. From conversations with nuclear plant specialists, suggestions were offered towards a more robust testbed for cable tests. This updated configuration includes cable tray sections, stressing bends in the test cable, feeding segments in conduit, and more realistic heating models for advanced aging. The updated configuration, taking into account all previously described changes except for improved heating models, is summarized in Figure 6.2.3. Cables will be tested with advanced aging protocol under this industrial settings testbed regime as well as with a control group tested without added stresses.

Initial accelerated aging tests focused on testing a wide range of instrumentation cables quickly enough to produce results and facilitate comparison of JTFDR to other more established methods. However, certain fallacies exist in this short time test. As explained in (54), a mathematical relationship exists between an accelerated aging time and a service life time based upon heating temperature and the activation energy. From further research, it has been determined that previous estimations of cable activation energy for cross-linked polyethylene (XLPE) at 1.33eV may be too high and a value of 1.25eV was deemed suitable. Similarly, the aging temperature may be too high to provide an accurate accelerated aging model. As such, a new set of

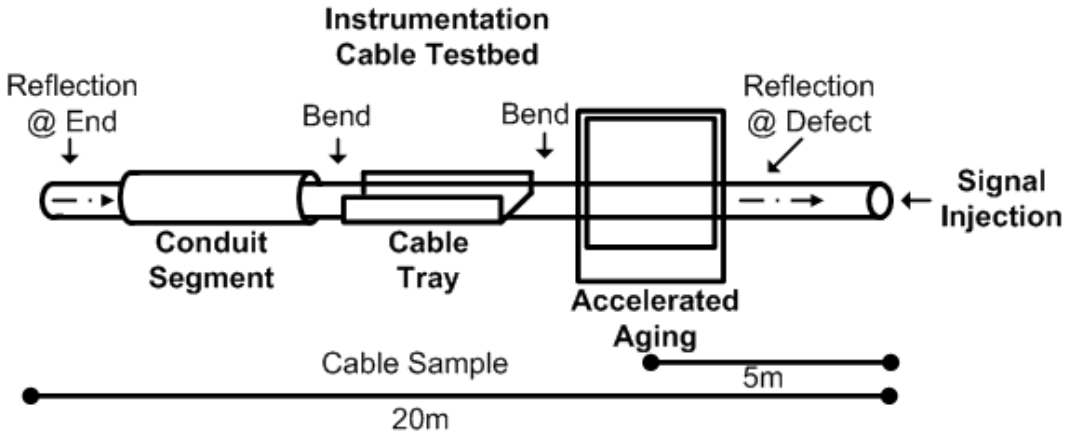

Figure 15: Experimental setup for Surface Wave Optimized JTFDR

parameters for accelerated aging for instrumentation level cable, such as a sample received from Swedish manufacturer Habia Cable, is presented in Figure 4. As further cable samples are received from IAEA member manufacturers in the United States and internationally, a homogenized or normalized baseline can be developed for nuclear instrumentation and future standards could be developed around JTFDR-based metrics where previously TDR or FDR metrics dominated.

6.3 Verifying Joint Time-Frequency Domain Reflectometry by Partial Discharge and High Voltage Assessment

6.3.1 Medium Voltage EPR and XLPE

Previously, a single sample of medium voltage tree-resistant cross-linked polyethylene cable (Prysmian/Pirelli MV-90 at 15kV) was tested using preliminary strategies of accelerated aging for verification of JTFDR methodology. To verify the capability of JTFDR to measure the life assessment of medium voltage cable, additional samples will be tested with longer and more involved accelerated aging processes. The aging temperature will be greatly reduced, and the activation energy for calculation of Arrhenius aging curve has been reduced. This results in a much longer experimental time, but the results should provide more realistic aging. Similar procedure follows for the aging of medium voltage and high voltage cable samples as previously outlined in Sections 4.3.1 and 4.3.3, including the cooling of cables after aging to verify that actual aging is measured instead of simply measuring geometric changes of the cables. However, the interval between periodic JTFDR metric assessment would likely be increased. Instead of performing periodic health assessments every hour of testing, it is suggested that the interval be 6 to 8 hours to provide 50 to 60 health assessment time-frequency cross correlation peak points. Higher voltage cable samples and additional samples with different insulation types should also be obtained and a summarizing table is provided in Table 4 for example proposed accelerated aging simulations. This table details additional tests for low voltage cable samples, represented here by the Habia RG-58 sample, continued and expanded accelerated aging tests for the previously tested tree-resistant cross-linked polyethylene (TR-XLPE) cable, and additional acquisition of a sample of 35kV ethylene propylene rubber (EPR) cable. Medium voltage cable samples from additional manufacturers may be tested as deemed necessary and initial quick assessment tests for all cable samples may be performed before each longer test to give a rough estimate of expected results.

Table 4: Summary of Cable Information and Experimental Duration

Insulation Type	Types of Cable	Activation Energy (eV)	Temp. (^{0}C)	Experimental Duration (Hr)
Cross-linked polyethylene (XLPE)	Habia, RG-58, 600 V	1.25	110	400
Tree-Resistant XLPE (TR-XLPE)	Prysmian, MV-90, 15 kV	1.30	110	360
Ethylene Propylene Rubber (EPR)	Prysmian, 35 kV	1.10	122	400

Additionally, a very low frequency (VLF), high voltage source has been acquired to perform additional verifying tests of JTFDR methodology. This source was chosen to provide a simpler and more cost-effective means of testing high voltage withstand and partial discharge than a comparable source at 50 or 60 Hz line frequency and provides options to test at 0.1, 0.05 and 0.02Hz. A high voltage withstand test can be performed on medium to high voltage cable with total capacitance between 0.1 to 6 μF and a voltage up to 50 kV. For additional verifying tests, a partial discharge generator and acquisition system was purchased to monitor high voltage partial discharges. This partial discharge unit operates within the same limits of the VLF source. Further research in high voltage tests will analyze the feasibility of using the acquired high voltage equipment to measure partial discharges in insulation by means of time-frequency or time-scale (wavelet) analysis.

6.3.2 High Temperature Superconducting Cable (HTS)

In order to further expand the use of JTFDR, use of the optimal reference and time-frequency methodology is suggested for an emerging cable type known as high temperature superconducting cable. High temperature

(a) (b)

Figure 16: Very low frequency source (VLF) operates at frequencies from 0.02-0.1Hz, simulating line frequency of 50 or 60 Hz, for high voltage tests up to 50kV with (a) controller, timer, and measurement unit and (b) high voltage tank capacitor

superconducting cable presents itself as an emerging technology in next generation power transmission, capable of high current capacity and reduced losses ideal for tie lines, DC bus interconnects, and general interchange between power utilities [38]. Superconducting materials are typically classified as ”high temperature” due to low resistivity at a critical temperature, TC, equal to or greater than the boiling temperature of liquid nitrogen (77K) though no definite temperature range is defined for this designation. Most high temperature superconducting implementations must be constantly cooled by a concentric coolant line [38, 39] to maintain low resistivity below a certain critical temperature.

Coolant temperatures for longer lengths of cable must be maintained with complex control systems that take hours or days to affect changes to overall coolant temperatures. Minor variations of temperature above the given critical temperature on either a global or localized scale could affect the safe and effective operation of HTS cable-based power transmission systems and increase the cable resistivity near the leakage inception point significantly. Thus, joint time-frequency domain reflectometry (JTFDR) is presented as a means of monitoring vital segments of such a cable technology or similar coolant fed emerging technologies. As such, non-destructive in-situ monitoring techniques could prove particularly useful in identifying localized variations in resistivity consistent with coolant leaks for implementation of real-time maintenance in smart grid applications.

Using example electrical properties from American Superconductor (AMSC), simulations have been accomplished to develop an optimal reference for HTS cable. These properties are used for simulation with a T_C equal to 91.2K. An amplified reference is then simulated for a distance up to 600 m using ADS transmission simulation software with a fault at 400 m. This fault is a simulation of localized coolant loss for a 1 m segment of cable accomplished by changing the impedance of this segment of cable with respect to the remaining cable segment.

The simulated injection of optimal reference is shown in Figure 18(a) with the reflection at the cable end point (600m). The cross correlation of the reference signal with the reflected signal is also shown in Figure 18(b) from which the coolant loss faulted segment can be seen at 400m. The designed and simulated optimal reference for HTS cable in transmission lengths of 600m should be 1.77MHz. Further research is proposed for HTS cable while I will be studying at Yonsei University, Korea in the spring of 2013 with proposals to be made to the Korea Electric Power Research Institute (KEPRI) and Korea Electric Power Corporation (KEPCO).

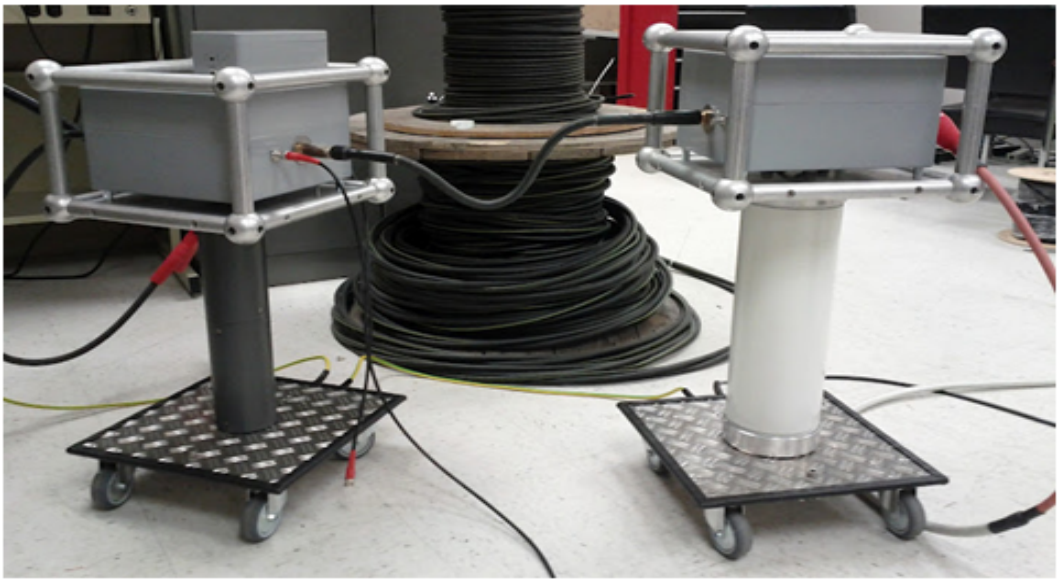

Figure 17: High voltage filter and partial discharge generator and measurement unit

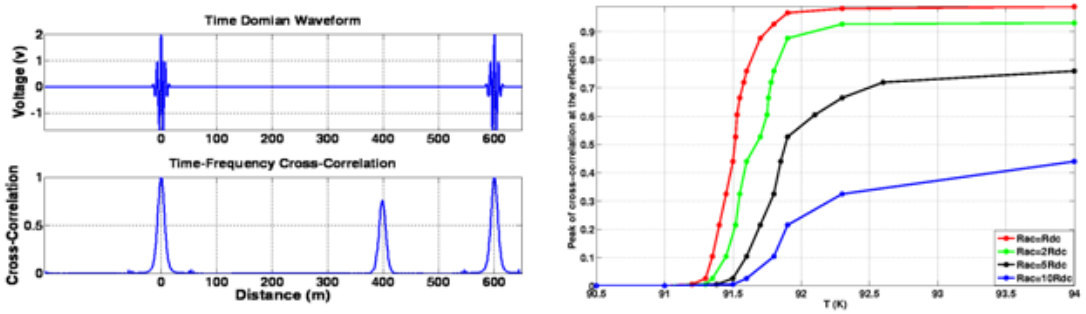

(a) (b)

Figure 18: (a) Optimal reference signal specified for HTS cable simulating a 600m segment faulted at 400m and (b) Cross correlation peaks for increasing resistance values used as an indication of cable health.

7 Conclusions

The proposed research provides a path toward comprehensive condition based maintenance for complex systems with interacting electrical and mechanical systems, such as motors, generators, wind turbine generators, and rotorcraft or aerospace systems. A Rényi entropy based mutual information metric is proposed for helicopter and general vibration-based health monitoring with the express goal of monitoring transient variations in signal components and creating statistic condition indicators based on these changes. Research on Joint Time-Frequency Domain Reflectometry in low voltage instrumentation cable samples provided by the International Atomic Energy Agency will help establish baselines for a variety of cables from manufacturers in the United States and other countries towards a goal of performance capability assessment in nuclear power plant recertification while we will continue to test the high voltage viability of the JTFDR method against verifying methods of high voltage test. As verification methods are underway, further assessment will be made into the use of JTFDR in measurement of partial discharge. This non-destructive reflectometry method has also been proposed to identify and locate localized impedance defects caused by changes in temperature in coolant filled high temperature superconducting (HTS) cable. These proposed works sum to the creation of a viable and prac-

tical implementation of non-invasive and non-destructive reflectometry-based cable health assessment. As CBM practices are implemented in both electrical cable systems and mechanical systems using similar time-frequency principles and metrics, a set of universal practices can be developed for health assessment.

8 Journal Publications

1. D. Coats, K. Cho, Y.J. Shin, N. Goodman, V. Blechertas, A.E. Bayoumi, “Advanced Time-Frequency Mutual Information Measures for Condition-Based Maintenance of Helicopter Drivetrains,” IEEE Transactions on Instrumentation and Measurement, vol.60, no.8, pp.2984-2994, Aug. 2011.

2. J. Wang, P.E.C. Stone, D. Coats, Y.J. Shin; R.A. Dougal; “Health Monitoring of Power Cable via Joint Time-Frequency Domain Reflectometry,” IEEE Transactions on Instrumentation and Measurement, vol.60, no.3, pp.1047-1053, March 2011.

8.1 In Progress

1. Hossein Mohammedpour, Moinul Islam, Mohd. Hasan Ali, David Coats, and Y.J. Shin, Dynamic Performance Comparison of Thyristor and Gate Controlled Series Capacitor, to be submitted to IEEE Transactions on Power Delivery.

2. David Coats, Md. Nazmul Alam, Qiu Deng, M. Ali, Yong-June Shin; “Joint Time-Frequency Optimized Reference for Surface Wave Reflectometry-Based Insulation Health Assessment;” to be submitted to IEEE Transactions on Electrical Insulation.

9 Conference Publications

1. David Coats, Md. Nazmul Alam, Qiu Deng, M. Ali, Yong-June Shin; “Joint Time-Frequency Optimized Reference for Surface Wave Reflectometry-Based Insulation Health Assessment”; The 11th International Conference on Information Science, Signal Processing and their Applications, July 2012.

2. Mohammed Hassan, David Coats, Yong-June Shin, Kareem Gouda, Abdel Bayoumi, “Quadratic-nonlinearity power-index spectrum and its application in condition based maintenance (CBM) of helicopter drive trains” Instrumentation and Measurement Technology Conference (I2MTC), 2012 IEEE International , vol., no., pp.1456-1460, 13-16 May 2012.

3. David Coats, Qiu Deng, Yong-June Shin; “Smart Grid Focused Joint Time-Frequency Health Assessment for High Temperature Superconducting Cables”; IEEE International Conference on Electronics, Information and Communication (February 2012).

4. David Coats; Hassan, M.A.; Goodman, N.; Blechertas, V.; Yong-June Shin; Bayoumi, A.; ,“Design of advanced time-frequency mutual information measures for aerospace diagnostics and prognostics,” Aerospace Conference, 2011 IEEE , vol., no., pp.1-8, 5-12 March 2011

5. David Coats, Jingjiang Wang, Yong-June Shin, Thomas Koshy, “Applications of Joint Time-Frequency Domain Reflectometry for Health Assessment of Cable Insulation Integrity in Nuclear Power Plants,” Proceedings of the 7th International Topical Meeting on Nuclear Plant Instrumentation, Control and Human Machine Interface Technologies (NPIC and HMIT 2010), November, 2010.

6. Jingjiang Wang, David Coats, Yong-June Shin, Thomas Koshy, “Applications of Joint Time-Frequency Domain Reflectometry for Health Assessment of Cable Insulation Integrity in Nuclear Power Plants,” International Symposium on the Ageing Management and Maintenance of Nuclear Power Plants (ISaG), Tokyo University, Tokyo, Japan, May 2010.

10 Graduate Coursework

Dept Prefix	Course Number	Course Title	Credit Hours	Grade
Undergrad				
MATH	544	Linear Algebra	3	A
ELCT	580	Audio Engineering	3	A
ELCT	564	RF Circuit Design for Wireless Communications	3	A
ELCT	572	Power Electronics	3	A
Graduate				
ELCT	551	Power System Design And Analysis	3	A
ELCT	563	Semiconductor Electronic Devices	3	B
ELCT	772	Advanced Power Electronics	3	B
ELCT	891B	Topic/Power and Energy Systems	3	A
ELCT	751	Advanced Power Systems Analysis	3	A
ELCT	837	Modern Control Theory	3	B
MATH	544	Wavelets	3	A
ELCT	752	Power Sys Grnd/Transients	3	A
ELCT	891A	Grid Connected Power Electronics	3	B+
ELCT	883	Power System Stability and Control	3	A
ELCT	891Q	Advanced Digital Signal Processing	3	A
ELCT	891D	Digital Controls	3	B
ELCT	797	Research	9	S
ELCT	899	Dissertation Preparation	3	
				Cumulative GPA
			45	3.591

References

[1] A. Bayoumi, et. al., "Integration of Maintenance Management Systems and Health Monitoring Systems through Historical Data Investigation," *Technical Specialists' Meeting on Condition Based Maintenance*, Huntsville, AL, 2008.

[2] A. Bayoumi, et al., "Implementation of CBM through the Application of Data Source Integration," *Technical Specialists' Meeting on Condition Based Maintenance*, Huntsville, AL, 2008.

[3] A. Bayoumi, et. al.,"Examination and Cost-Benefit Analysis of the CBM Process," *Technical Specialists' Meeting on Condition Based Maintenance*, Huntsville, AL, 2008.

[4] A. Bayoumi, et. al., "Aircraft Components Mapping and Testing for CBM," *Technical Specialists' Meeting on Condition Based Maintenance*, Huntsville, AL, 2008.

[5] Ignacio Santamaría-Caballero, Carlos J. Pantaleón-Prieto, Jesús Ibáñez-Díaz, Enrique Gómez-Cosío, "Improved procedures for estimating amplitudes and phases of harmonics with application to vibration analysis," *IEEE Transactions on Instrumentation and Measurement*, vol. 47, no. 1, Feb. 1998, pp. 209 - 214.

[6] Giovanni Betta, Consolatina Liguori, Alfredo Paolillo, Antonio Pietrosanto, "A DSP-based FFT-analyzer for the fault diagnosis of rotating machine based on vibration analysis," *IEEE Transactions on Instrumentation and Measurement*, vol. 51, no. 6, Dec. 2002, pp. 1316 - 1322.

[7] Jaidilson Jó da Silva, Antonio Marcus Nogueira Lima, Franz Helmut Neff, José Sérgio da Rocha Neto "Non-invasive fast detection of internal fouling layers in tubes and ducts by acoustic vibration analysis," *IEEE Transactions on Instrumentation and Measurement*, vol. 58, no. 1, Jan. 2009, pp. 108 - 114.

[8] Paul Grabill, Jason Seale, Dariusz Wroblewski, Tom Brotherton. "iTEDS: the intelligent Turbine Engine Diagnostic System" *48th International Instrumentation Symposium*, pp. 6.

[9] Marc Vedrines, Vincent Gassmann, Dominique Knittel, "Moving web-tension determination by out-of-plane vibration measurements using a laser," *IEEE Transactions on Instrumentation and Measurement*, vol. 58, no. 1, Jan. 2009, pp. 207 - 213.

[10] Ruqiang Yan, Robert X. Gao, "Complexity as a measure for machine health evaluation," *IEEE Transactions on Instrumentation and Measurement*, vol. 53, no. 4, Aug. 2004, pp. 1327 - 1334.

[11] J. Banks, T. Bair, K. Reichard, D. Blackstock, D. McCall, J. Berry, "A Demonstration of a Helicopter Health Management Information Portal for U.S. Army Aviation," *Proceedings of the IEEE Aerospace Conference*, Big Sky, MT 2005. pp. 3748-3755.

[12] S. Santhi, V. Jayashankar, "Time-frequency analysis method for the detection of winding deformation in transformer," *Proceedings of the IEEE Transmission and Distribution Conference and Exposition*, Chicago, IL, 2008. pp. 1-5.

[13] S. B. Dalal, R. S. Gorur, "Aging of Distribution Cables in Service and Its Simulation in the Laboratory," *IEEE Transactions on Dielectrics and Electrical Insulation*, Vol. 12 No. 1, Feb. 2005.

[14] Satish Rajagopalan, José A. Restrepo, José M. Aller, Thomas G. Habetler, Ronald G. Harley, "Nonstationary motor fault detection using recent quadratic time frequency representations," *IEEE Transactions on Industry Applications*, vol. 44, no. 3, May/Jun. 2008, pp. 735 - 744.

[15] Kwang Ik Cho, David Coats, John Abrahms, Nicholas Goodman, Yong-June Shin, Abdel Bayoumi, "Applications of Time-Frequency Analysis for Aging Aircraft Component Diagnostics and Prognostics," *Proceedings of SPIE-Advanced Signal Processing Algorithms, Architectures, and Implementations XVIII*, San Diego, CA, July 2008.

[16] Andrew R. Scott, "Characterizing system health using modal analysis," *IEEE Transactions on Instrumentation and Measurement*, vol. 58, no. 2, Feb. 2009, pp. 297 - 302.

[17] Ruqiang Yan, Robert X. Gao, "Hilbert-Huang transform-based vibration signal analysis for machine health monitoring," *IEEE Transactions on Instrumentation and Measurement*, vol. 55, no. 6, Dec. 2006, pp. 2320 - 2329.

[18] T. Cover and J. Thomas, Elements of Information Theory New York: Wiley, 1991.

[19] D. Coats, K. Cho, Y.J. Shin, N. Goodman, V. Blechertas, A.E. Bayoumi, "Advanced Time-Frequency Mutual Information Measures for Condition-Based Maintenance of Helicopter Drivetrains,"*IEEE Transactions on Instrumentation and Measurement*, vol.60, no.8, pp.2984-2994, Aug. 2011.

[20] W. J. Williams, M. L. Brown, and A. O. Hero, "Uncertainty, information, and time-frequency distributions," in *Proceedings of SPIE-Advanced Signal Processing Algorithms, Architectures, and Implementations X*, vol. 1566, 1991, pp. 144-156.

[21] T.-H. Sang and W. J. Williams, "Rényi information and signal-dependent optimal kernel design," in *Proc. IEEE Int. Conf. Acoustics, Speech, and Signal Processing ICASSP* '95, vol. 2, 1995, pp. 997-1000.

[22] L. Cohen, "*Time-Frequency Signal Analysis*," Prentice Hall, New York, 1995.

[23] Leon Cohen, "Time-frequency distributions - a review," *Proceedings of the IEEE*, Vol.77, July, 1989, pp. 941-981.

[24] R.G. Baraniuk, P. Flandrin, A. Janssen, and O. Michel, "Measuring time-frequency information content using the Renyi Entropies," *IEEE Transactions on Information Theory*, vol. 47, no. 4, May 2001, pp 1391-1409.

[25] Yong-June Shin, E. J. Powers, and W. M. Grady, "On definition of cross time-frequency distribution function," *Proceedings of SPIE-Advanced Signal Processing Algorithms, Architectures, and Implementations X*, San Diego, CA, July 2000. pp. 9-16.

[26] Bin Zhang, et al, "Application of blind deconvolution denoising in failure prognosis," *IEEE Transactions on Instrumentation and Measurement*, vol. 58, no. 2, Feb. 2009, pp. 303 - 310.

[27] *IEEE Standard*-1064-1991, "Guide for Multifactor Stress Functional Testing of Electrical Insulation Systems," 1991.

[28] Michael E. Stieber, Emil Petriu, George Vukovich, "Instrumentation architecture and sensor fusion for systems control," *IEEE Transactions on Instrumentation and Measurement*, vol. 47, no. 1, Feb. 1998, pp. 108 - 115.

[29] Stephen C. Stubberud, Kathleen A. Kramer, "Data association for multiple sensor types using fuzzy logic," *IEEE Transactions on Instrumentation and Measurement*, vol. 55, no. 6, Dec. 2006, pp. 2292 - 2303.

[30] Y. J. Shin, E. J. Powers, T. S. Choe, C. Y. Hong, E. S. Song, J. G. Yook, J. B. Park, "Application of Time-Frequency Domain Reflectometry for Detection and Localization of a Fault on a Coaxial Cable," *IEEE Transactions on Instrumentation and Measurement*, Vol. 54, No. 6, Dec. 2005.

[31] J. Wang, P. Crapse, Y. J. Shin, and R. Dougal, "Diagnostics and Prognostics of Electric Cables in Ship Power Systems via Joint Time-Frequency Domain Reflectometry," *Proceedings of the IEEE Instrumentation and Measurement Technology Conference*, May 2008, pp. 917-921.

[32] J. Wang, P. Crapse, Y. J. Shin, and R. Dougal, "Diagnostics and Prognostics of Electric Cables in Nuclear Power Plants via Joint Time-Frequency Domain Reflectometry," *IEEE International Symposium on Electrical Insulation*, Jun. 2008, pp. 24-27.

[33] J. Wang, P.E.C. Stone, D. Coats, Y.J. Shin; R.A. Dougal; , "Health Monitoring of Power Cable via Joint Time-Frequency Domain Reflectometry," *Instrumentation and Measurement, IEEE Transactions on*, vol.60, no.3, pp.1047-1053, March 2011.

[34] L. Cohen, "Time-frequency distributions - a review," *Proc. IEEE*, Vol.77, pp. 941-981, July, 1989.

[35] L. Cohen, "*Time-Frequency Signal Analysis*," Prentice Hall, New York, 1995.

[36] Rothwell, E.J.; "Exponential Approximations of the Bessel Functions I0,1(x), J0,1(x), Y0(x), and H01,2(x), with Applications to Electromagnetic Scattering, Radiation, and Diffraction [EM Programmer's Notebook]" *Antennas and Propagation Magazine, IEEE* no. 3 pp.138-147, June 2009

[37] Millane, R.P., Eads, J.L; "Polynomial approximations to Bessel functions" *Antennas and Propagation, IEEE Transactions on* vol. 51, no. 6, pp. 1398-1400, June, 2003

[38] Wei Pi, Yinshun Wang, Lei Chen, and Chengrong Li, "Numerical Study of Current Distribution and Stability of LTS/HTS Hybrid Superconductor," *IEEE Transactions on Applied Superconductivity*, vol. 20, no. 3, pp. 2180-2183, June 2010.

[39] T. Takahashi, H. Suzuki, M. Ichikawa, T. Okamoto, S. Akita, S. Maruyama, and A. Kimura, "Dielectric Properties of 500 m Long HTS Power Cable," *IEEE Transactions on Applied Superconductivity*, vol. 20, no. 3, pp. 1767-1770, June 2005.